ELSEVIER

Marine and Petroleum Geology 18 (2001) 411–439

Marine and Petroleum Geology

www.elsevier.com/locate/marpetgeo

Structural core analysis from the Gullfaks area, northern North Sea

J. Hesthammer[a,*], H. Fossen[b]

[a]Statoil, N-5020 Bergen, Norway
[b]Department of Geology, University of Bergen, Allegt. 41, N-5007 Bergen, Norway

Received 4 October 1999; received in revised form 28 August 2000; accepted 6 October 2000

Abstract

Comprehensive analyses of more than 8 km of core data from the Gullfaks area, northern North Sea, have proven invaluable for a thorough understanding of the detailed deformation characteristics. In addition, the integration of the results with analyses of dipmeter data, well log correlation data, seismic data and field analogue data yields important information on the general structural characteristics and reservoir properties.

Microanalyses show that all faults in the reservoirs are associated with abundant shear bands (deformation bands) clustered in a narrow damage zone that seldom exceeds a few tens of metres in width. Where mica is abundant, the bands are dominated by phyllosilicate framework structures, whereas disaggregation structures dominate cleaner sandstones. Permeability reduction across the shear bands depends on the amount of phyllosilicates present and is generally negligible in clean sandstones. Only minor amounts of cataclasis are observed. The width of the shear bands increases with increasing grain size.

Orientation analyses of the dip of shear bands associated with minor faults show that these are symmetrical around a vertical axis. Since the general bedding rotation as observed in well data and seismic data is 10° towards the west, most shear bands must have formed after the rotation of bedding. This is likely because minor faults formed as (late) accommodation structures during slip along the main faults.

The reservoir rocks are affected ductilely (by fault drag) in a zone wider than that affected by shear bands. This shows that part of the deformation was by a homogeneous redistribution of individual grains rather than by shear bands or discrete faulting. The integrated analyses of core data with seismic data demonstrate that most (curvi-)linear and fault-like features observed on seismic attribute maps are in fact noise-related.

Keywords: Structural core analysis; Gullfaks area, northern North Sea; Deformation bands

1. Introduction

Development of structurally complex oil and gas fields demands a thorough understanding of reservoir characteristics in order to optimise field performance. This requires integrated analyses and understanding of all available data. A series of articles from the Gullfaks Field demonstrate how the integration of dipmeter data, well log correlation data and reflection seismic data has helped in constraining the structural geology of the Gullfaks Field (Fossen & Hesthammer, 1998a; Hesthammer, 1998, 1999a; Hesthammer & Fossen, 1997a,b, 1998, 2000). *Seismic data* provide important information on the general structural geology of an area such as overall fault geometry and bedding dip. However, due to abundant seismic noise, the interpreter is challenged to separate real features from seismic artefacts. *Well log correlation data* help to constrain the seismic interpretation by allowing coupling of seismic reflections and reservoir zonation data. *Dipmeter data* enable the geologist to confirm that seismically observable features such as faults and bedding dip are real. In addition, dipmeter data help to tie interpretations from the seismic into the subseismic domain and reveal information on subseismic faults and changes in bedding dip. On the Gullfaks Field, dipmeter data have helped separating seismic noise from real features. *Core data* represent the most detailed information available and are useful for quality control of observations from well data and seismic data in addition to providing important information on reservoir properties.

Today, most oil and gas companies carry out detailed structural core analyses for reservoir development purposes. However, most such studies are limited to analyses of (a) the fault zone (width, shale content, brecciation), and (b) petrophysical parameters (permeability and porosity) and spatial distribution (fracture frequency) of shear bands in the

* Corresponding author. Tel.: +475599-2130; fax: +47-55992097.
E-mail addresses: jonhe@statoil.com (J. Hesthammer), haakon.fossen@geol.uib.no (H. Fossen).

0264-8172/01/$ - see front matter
PII: S0264-8172(00)00068-4

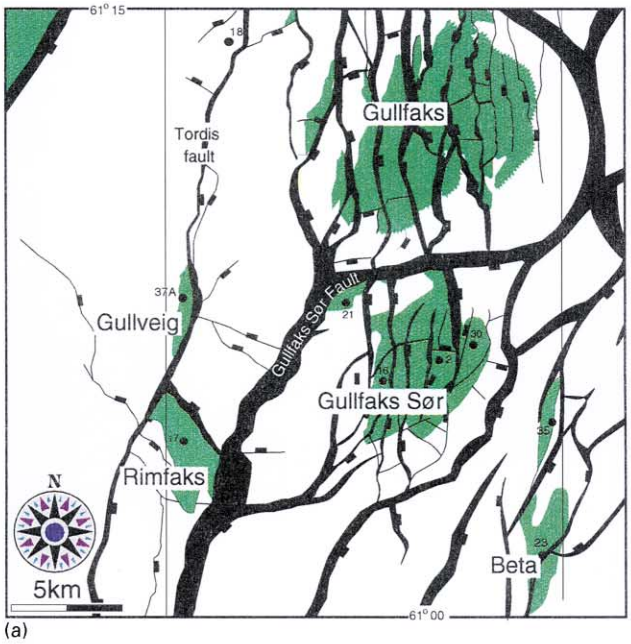
61° 15
Gullfaks
Tordis fault
Gullfaks Sør Fault
Gullveig
Gullfaks Sør
Rimfaks
Beta
N
5km
61° 00

(a)

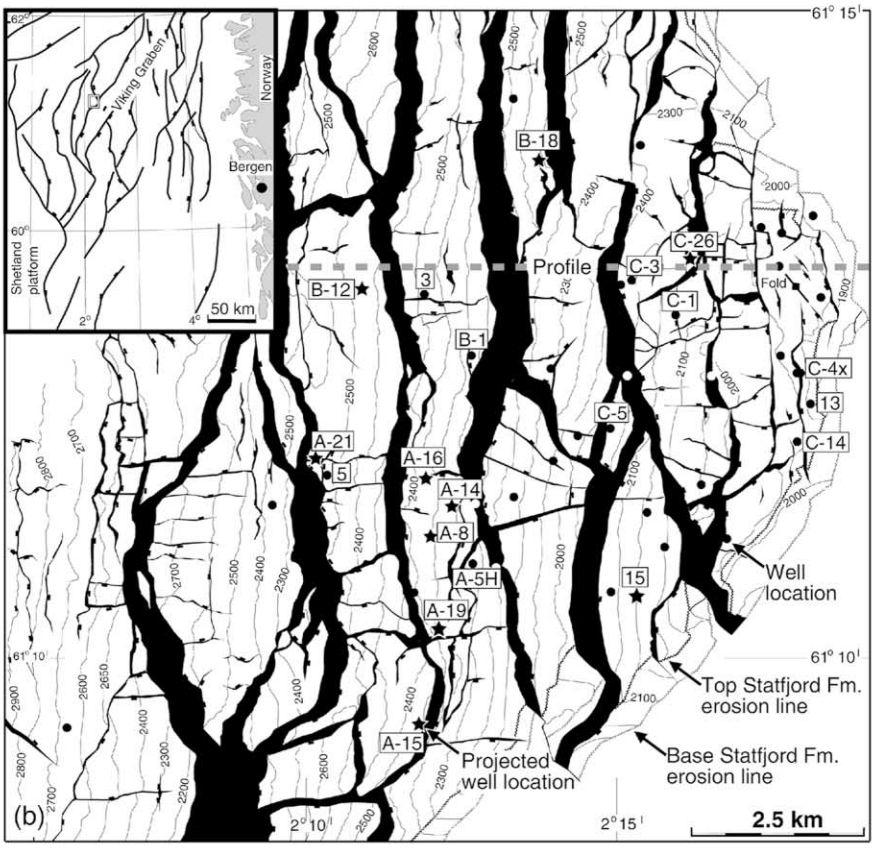
Viking Graben
Norway
Bergen
Shetland platform
50 km
61° 15
B-18
B-12
B-1
Profile
C-26
C-3
C-1
Fold
C-4x
C-5
C-14
A-21
A-16
A-14
A-8
A-5H
A-19
A-15
Well location
Top Statfjord Fm. erosion line
Base Statfjord Fm. erosion line
Projected well location
61° 10
2° 10
2° 15
2.5 km

(b)

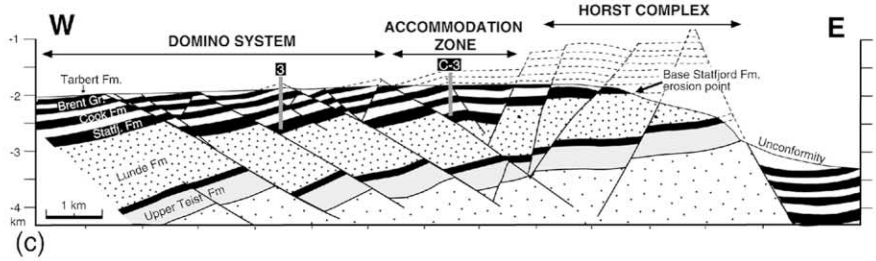
W
E
DOMINO SYSTEM
ACCOMMODATION ZONE
HORST COMPLEX
Tarbert Fm.
Brent Gr.
Cook Fm.
Statfj. Fm.
Lunde Fm.
Upper Teist Fm.
Base Statfjord Fm. erosion point
Unconformity
1 km
km

(c)

damage zone. These data are used for calculating fault seal potential to be used in reservoir models by applying the parameters to seismically interpreted faults. But core data also allow for orientation analyses of structural bedding dip, faults and shear bands. This provides the geoscientist with a fuller understanding of subseismic geometries of faults and bedding in addition to verifying seismic observations. As will be demonstrated in this work, such an integrated approach reveals important findings that must be considered when trying to model field performance. The failure to do so may lead to erroneous results and non-optimal field development.

The present study focuses on how structural analyses of more than 8 km of core data from the Gullfaks area yield additional important information on fault sealing characteristics, timing of deformation, deformation types and geometry of fault zones. The work is organised as follows. Section 2 introduces the reader to the Gullfaks Field. Section 3 describes the methodology used for structural core analysis. Section 4 gives a description of the fractures. Section 5 discusses the results on individual basis. Section 6 discusses the results in view of other data (seismic data and well data) and models for reservoir performance. As the results from the analyses demonstrate large variations in individual fault characteristics, it has not been the purpose of this work to build better reservoir modelling tools, but to increase the readers awareness of the structural characteristics and associated variability contained in the reservoir rocks in the Gullfaks area.

2. The Gullfaks area

The cores studied are mostly collected from the Gullfaks Field (6.077 km) whereas some additional cores (2.048 km) are from the neighbouring satellites (Gullfaks Sør, Gullveig, Rimfaks and Gamma) (Fig. 1). The Gullfaks Field, situated in block 34/10 along the western flank of the Viking Graben (Fig. 1), occupies the eastern half of a 10–25 km wide fault block and is bounded by large-scale faults with kilometre-scale offsets. The Gullveig and Rimfaks satellites west of the main field form the westward and southward continuation of the Gullfaks structure in an area of less extensional strain. Gullfaks Sør covers a major part of a 10 km wide fault block south of the Gullfaks Field, from which it is separated by a ~1 km fault. In the following, the term Gullfaks area is used as a common expression for the Gullfaks Field and the satellites.

The area has been affected by at least two major rift phases (e.g. Gabrielsen, Færseth, Steel, Idil, & Kløvjan, 1990; Roberts, Yielding, & Badley, 1990). The first phase occurred in the Permian and Early Triassic and affected the total width of the northern North Sea, whereas the second, late Jurassic, rift phase was more localised to the central portions of the northern North Sea (e.g. Færseth et al., 1995).

More than 200 wells have been drilled in the Gullfaks area since production started from the Gullfaks Field in 1985. In addition to standard well data (log data containing gamma ray, resistivity, neutron/density and sonic velocity measurements), ~40 km of dipmeter data and more than 8 km of core data have been collected for detailed stratigraphic and structural studies.

2.1. Stratigraphy

The lowermost strata penetrated by wells in the Gullfaks area comprise interbedded sandstones, claystones and shales of the Triassic Hegre Group (Fig. 2). The sediments were deposited in a continental environment. Alluvial sandstones of the Rhaetian–Sinemurian Statfjord Fm. overlie the Hegre Group. Overlying this sequence are Sinemurian–Toarcian marine clay- and siltstones of the Amundsen Fm., regressive, marine, silty claystones, muddy sandstones and sands of the Cook Fm., and marine shales and siltstones of the Drake Fm. The Bajocian–Early Bathonian Brent Group forms the uppermost part of the reservoir. The Brent Group was deposited in a deltaic environment and comprises sandstones of the Broom, Rannoch and Etive Fms, interbedded sandstones, shales and coals of the Ness Fm. and excellent reservoir quality sandstones of the Tarbert Fm.

The reservoir rocks in the Gullfaks area are capped by Cretaceous shales and siltstones. An unconformity, representing a time gap of up to 100 My, defines the base of the Cretaceous sediments. The Cretaceous strata post-date the major part of the faulting history of the Gullfaks area. Locally, up to 100 m of the Upper Jurassic Heather Fm. is preserved in the hanging walls to the main N–S trending faults on the main field, and more than 1 km in the Gullfaks Sør area.

2.2. Structural geology

A general description of the structural geology of the Gullfaks Field is given by Fossen and Hesthammer (1998a). In general, the Gullfaks Field is separated into three structural domains: a western domino-style system with east-dipping faults and west-dipping strata; a deeply eroded eastern horst complex of subhorizontal strata and steep faults; and a transitional accommodation zone (graben system) which is in part identified as a modified anticlinal fold (Fig. 1). Seismic mapping has revealed a similar geometrical constellation on Gullfaks Sør to the south.

Fig. 1. (a) Structure map of the Gullfaks area. (b) Structure map of the Statfjord Fm. in the Gullfaks Field with location of wells discussed in text; see inset map for location. Star symbols indicate location of wells projected down from shallower reservoir levels. (c) E–W profile through the three different structural domains — see (b) for location. Modified after Fossen and Hesthammer (1998a).

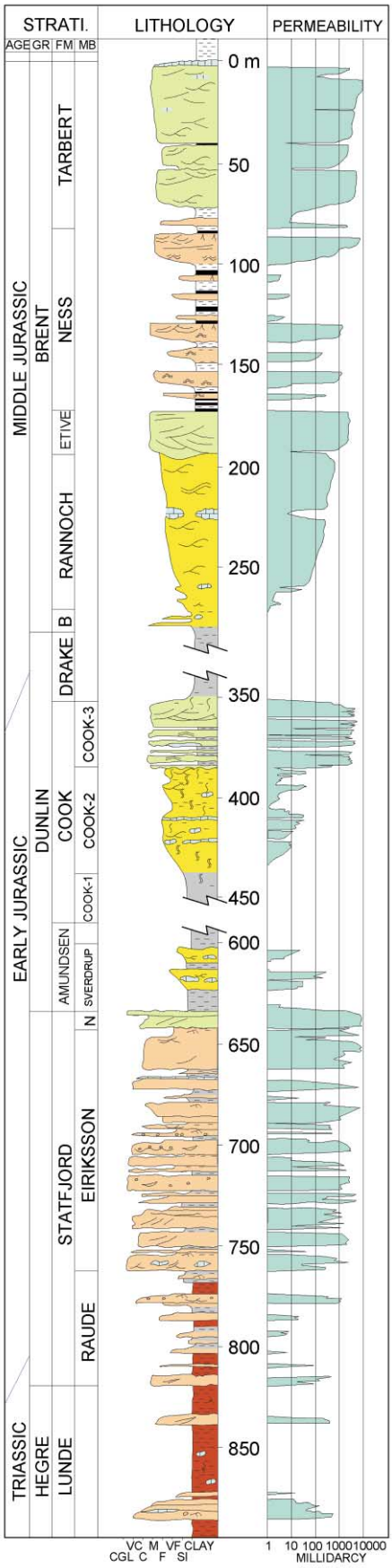

Fig. 2. Stratigraphic column for the Jurassic and Triassic reservoir units within the Gullfaks Field. Modified after Tollefsen, Graue, and Svinddal (1994).

The west-dipping domino faults exhibit displacements up to 500 m. The faults dip 25–30° to the east, whereas the bedding has an average dip of 15° to the west. The faults show increasing complexity ("branching") towards higher reservoir levels. Several E–W trending minor faults with offsets less than 50 m compartmentalise the domino fault blocks, and are believed to be related to internal block deformation during differential slip along the main faults (Fossen & Rørnes, 1996). Kilometre-scale drag (termed "large-scale") expressed as a gentle hanging-wall syncline causes bedding dip to decrease in a westerly direction. The effect of this drag is greater at shallower reservoir levels. Good agreement between various kinds of well data and seismic data shows that this is not an artefact in the seismic data prior to depth-conversion). The horst complexes in both Gullfaks Sør and the Gullfaks Field are characterised by poorer seismic data quality, which complicates the interpretation. Seismically observable faults generally display much steeper dips than that observed within the domino system. Bedding within the horst complexes is mainly sub-horizontal or gently east-dipping. The accommodation zone on the Gullfaks Field (Fig. 1b) is bounded by steep (65°) faults to the east and lower-angle (25°) faults to the west. The zone is identified as a collapsed anticline with a west-dipping western limb and a sub-horizontal eastern limb.

The Gullveig satellite is located in the footwall to a N–S striking fault and forms a continuation of the Gullfaks Field to the west. The fault density is lower in this area than in both Gullfaks Sør and the Gullfaks Field. Rimfaks is located in the southwestern continuation of the Gullfaks Field, whereas Gamma is positioned in a deeper fault block closer to the Viking Graben.

3. Methodology

Most approaches to structural core analyses are designed to answer specific questions such as how many faults and shear bands that exist in the reservoir, the width of the damage zones and fault zones, the permeability and porosity reduction associated with shear bands and fault zones, and deformation mechanisms. The results are typically used as input in models for reservoir performance. The present study is different in that its purpose is to enhance our general understanding of small-scale reservoir characteristics, not only sealing capacity of faults. This demands a different approach to the analysis. Instead of defining a few needed parameters, it was desirable to collect information on all the different parameters that could be investigated and measured from the cores. As this work will demonstrate, such studies are important and reveal information that was not thought of prior to the study and that may render existing

modelling tools useless due to parameters that were not thought of in the more dedicated studies.

All cores from the Gullfaks area were slabbed so as to display the highest dip of bedding, and three different cuts are available for analysis. The A-cut is used for mineralogical and petrophysical studies, the central B-cut is used for sedimentological and structural analyses and the C-cut is preserved undisturbed. The B-cut is typically glued onto a base or submerged in epoxy. For general structural studies, evaluation of the B-cut is sufficient. However, for fault seal evaluation, it is often necessary to use the A-cut for investigations of reduction in permeability and porosity, as well as for SEM analyses and studies of thin sections. In addition, the central B-cut may be too thin for detailed analyses of fault orientation or, if submerged in epoxy, the only possibility for evaluating fault orientation is through investigation of the A- or C-cuts.

For detailed and general structural analyses of core data, it is necessary to collect information about petrophysical properties, mineralogy, sedimentology, fracture geometries and characteristics, movement indicators and bedding orientation (e.g. Aarland & Skjerven, 1998; Gabrielsen & Kløvjan, 1997; Gabrielsen & Koestler, 1987). Fig. 3 summarises the type of information needed for a thorough structural investigation (see also Gabrielsen, Aarland, & Alsaker, 1998 for discussion on fracture description).

Collected information should also include stratigraphic level and measured depth in the well (transformable to true vertical depth). Furthermore, changes in bedding orientation with respect to the borehole wall may yield information on general deformation characteristics such as drag (Hesthammer, 1998). Description of the rock type includes sedimentary structures, grain size and mineralogy. This information is important for statistical analyses of hardness, width and type of fractures, as will be demonstrated later.

For the specific fractures, it is important to collect information about displacement and to separate faults, joints and veins. The type of fracture (open, disaggregation structure, grain size reduction, phyllosilicate framework, phyllosilicate smear, sand injection or mineral filled) yields important information on sealing potential. The geometric description should record whether the fracture is planar or curved, single/anastomosing or within complex network zones, and the degree of connectivity. The connectivity of a fracture refers to how many other fractures intersect the investigated structure. When the connectivity exceeds five, it is generally more convenient to group the fractures into a network zone where the number of fractures within the zone is described. Orientation data should record information on the angle between the intersection of the fracture with the slabbed core surface and bedding, and whether the intersection line dips in the same or opposite direction of the bedding. In addition, for complete 3D orientation analyses, it is necessary to collect information on the angle between the fracture and the section oriented perpendicular to the slabbed core surface (Fossen & Hesthammer, 2000; Hesthammer & Henden, 2000a). If the fracture is associated with drag, the width of the drag zone and the change in dip of bedding should be recorded. The width of the fracture is important for measurements of sealing potential. The colour of the fracture with respect to the host rock helps the interpreter to distinguish between different types of fractures. The same applies to differences in hardness between the fracture zone and the host rock. If movement indicators are present, it may be possible to study fault kinematics or paleostress.

It is also necessary to collect information on missing sections that may be connected to poor coherence or tectonical fragmentation. General information from well log analyses such as identification of larger-scale faults and associated missing section, permeability, porosity and studies of dipmeter data help to relate observations from fracture studies to the overall geology. Cores can easily fracture as a result of handling and release of pressure, and any relevant information on the core handling procedures and collection method should be recorded. It may also be important to obtain information on the proximity to large-scale structures such as faults that do not penetrate the well but may influence on the cored rocks.

All cores from the Gullfaks Field contain abundant bedding-parallel open fractures. It is likely that most of these developed during collection due to the pressure release that occurs when the cores are elevated from reservoir levels (at approximately 2 km depth) to the surface. In addition, many intervals contain open fractures that are subparallel to the borehole wall. Where the wells are subvertical, it is often not possible to determine if the fractures developed as a result of torque during sampling or if they result from pressure release in the reservoir (unless the fractures are highly undulating or show evidence of plumose jointing). Since cores from non-vertical wells on the Gullfaks Field do not contain systematic open fractures that indicate vertical jointing in the reservoir, a feature that may apply to many more oil and gas fields in the North Sea (Gabrielsen et al., 1998), it is likely that the vertical fractures observed in cores from vertical wells are caused by the core sampling procedures. Therefore, structural core analyses on the Gullfaks Field are only carried out for those fractures that show clear indications of being developed as a result of geological deformation. This includes fractures that contain displacement indicators (i.e. faults) as well as other closed fractures (shear bands and veins). Open fractures without indications of slip are not included in this study.

4. Description of fractures

4.1. Geometries and appearances

By far the most abundant fractures observed on the Gullfaks Field, with the exception of bedding-parallel joints, are microfaults in the form of shear bands or

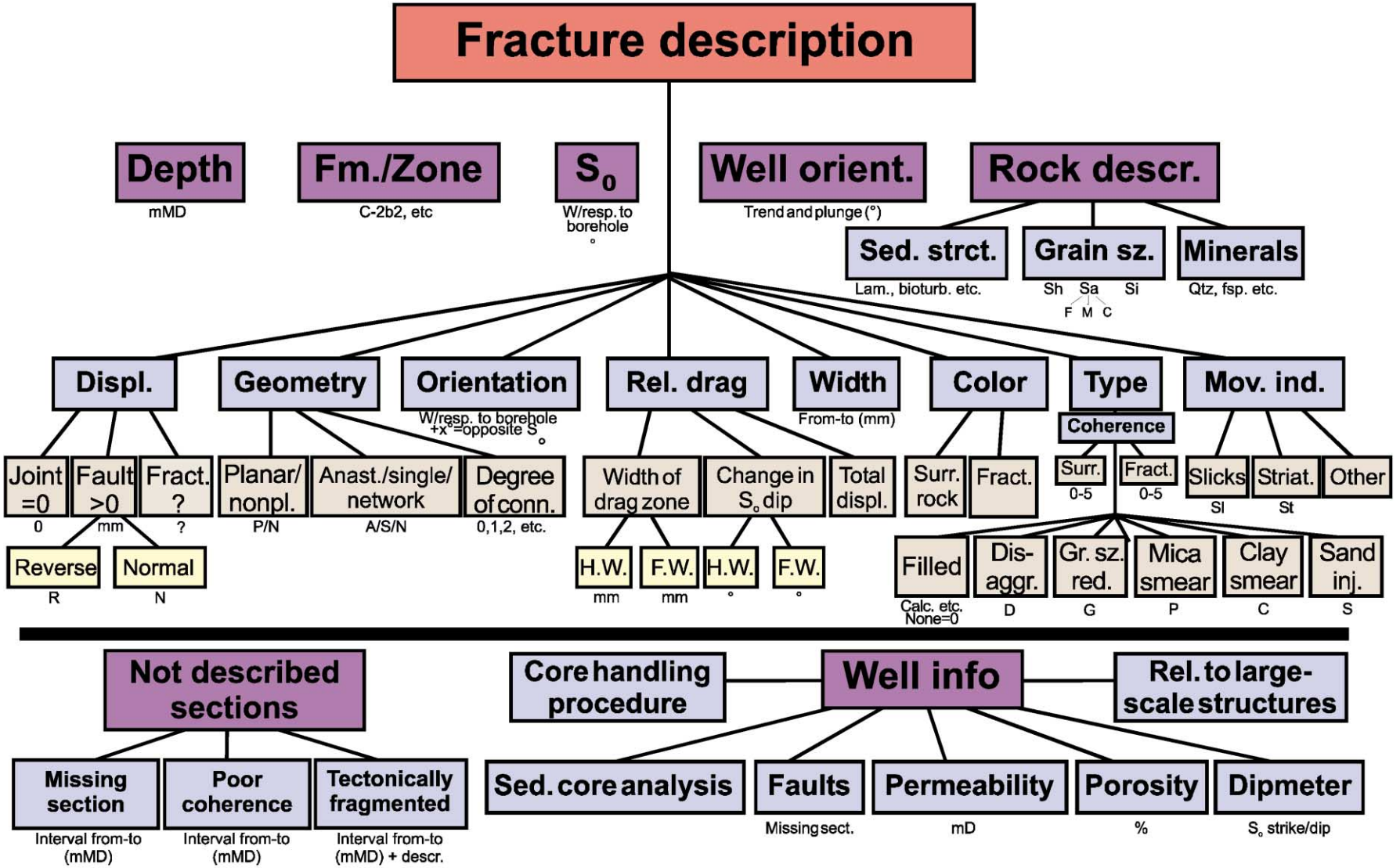

Fig. 3. A comprehensive structural analysis of core data is based on a complete data collection. This includes geometric and physical properties of the fractures and surrounding rocks, bedding and fracture orientation, well log information, sedimentology, intervals not described and core handling procedures.

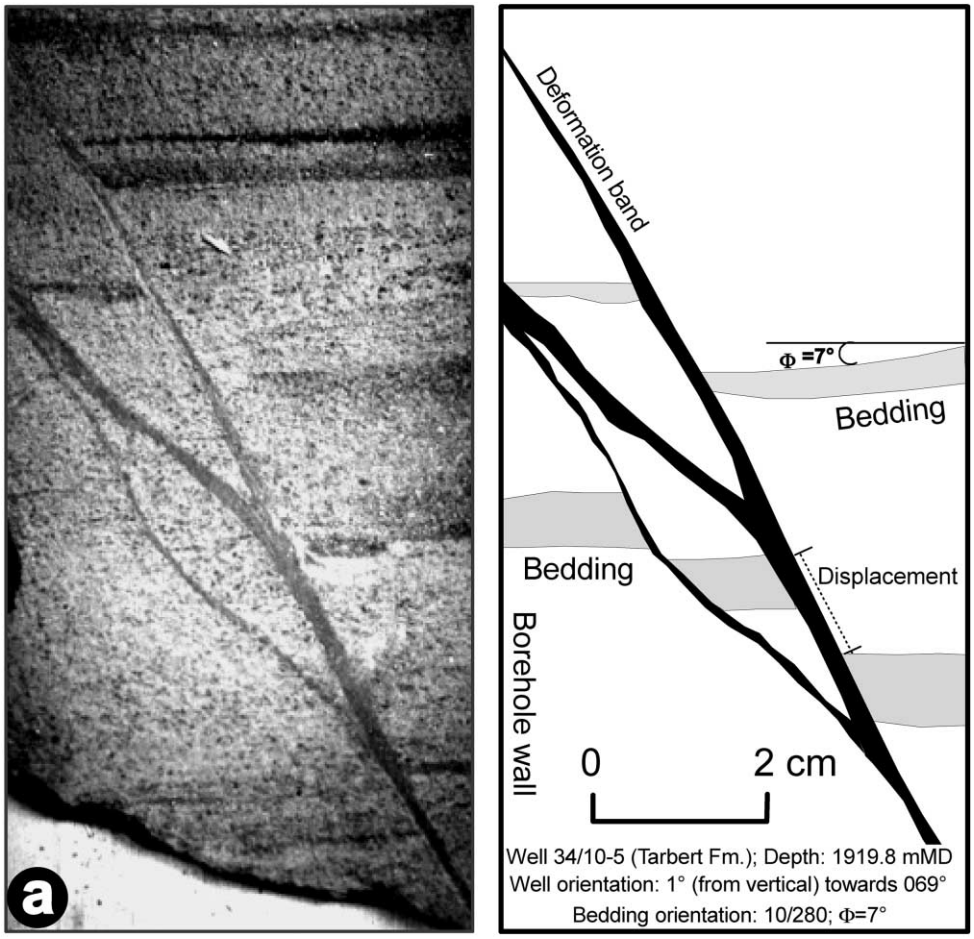

Fig. 4. (a) Deformation bands observed in cores from the Tarbert Fm. in the vertical exploration well 34/10-5. The fractures are associated with phyllosilicate framework, disaggregation structures and minor amounts of cataclasis. One of the bands is planar whereas the other two are curved. The connectivity for all three structures is two. No discrete slip surface has developed. (b) A fault with discrete slip surface and 6 m displacement penetrates rocks of the Ness Fm. in well 34/10-A-15. Surrounding the fault are abundant shear bands with less than a few centimetres offset. (c) A fault associated with 69 m missing section was penetrated by well 34/10-B-12. The fault zone is associated with a breccia. Abundant shear bands exist in a damage zone near the fault.

deformation bands (e.g. Antonellini & Aydin, 1994, 1995; Antonellini, Aydin, & Pollard, 1994; Aydin, 1978; Aydin & Johnson, 1978, 1983; Fossen & Hesthammer, 1997, 1998b). In this study, the term shear band is used for all closed bands without a discrete slip surface, whereas the term deformation band more specifically refers to shear bands in quartzose porous sandstones (Aydin, 1978; Fowles & Burley, 1994; Harris, Taylor, & Walper, 1960; Jamison, 1982; Pittman, 1981; Underhill & Woodcock, 1987; Wibberley, Petit, & Rives, 1999). Shear bands are typically thin (millimetre-thick) shear zones with less then a few centimetres displacement. Shear bands are usually associated with reduction in permeability (Antonellini & Aydin, 1994; Gabrielsen et al., 1998; Gabrielsen & Koestler, 1987), depending on the amount of cataclasis and phyllosilicate content, and therefore act as barriers to fluid flow (Harper & Lundin, 1997). Shear bands in Utah (most previous studies) developed after the rocks were buried and consolidated and are typically associated with large amounts of cataclasis. Shear bands in the Gullfaks area developed in little consolidated rocks and are mainly associated with grain reorganisation and reorganisation of phyllosilicate minerals. These differences will affect both petrophysical parameters and geometry of the deformation structures.

Studies of deformation bands in Utah and elsewhere show that they occur as (a) isolated structures, (b) linked systems, (c) complex zones of multiple interconnected bands, and (d) in a zone at either side of a fault, where the fault is defined by a discrete, polished slip surface (Aydin & Johnson, 1978, 1983; Fossen & Hesthammer, 1997, 1998b). It is likely that these types are associated with stages in development by increasing strain through time from a single deformation band to a fault containing a distinct slip surface (note that a distinction is drawn throughout this work between shear/deformation bands and faults). During this process, displacement increases from a few millimetres to a few centimetres in stage (a) to (b). Stage (c) is typically associated with cumulative offsets up to a few tens of centimetres, whereas the fault typically has developed several metres displacement at stage (d). Prior to the development

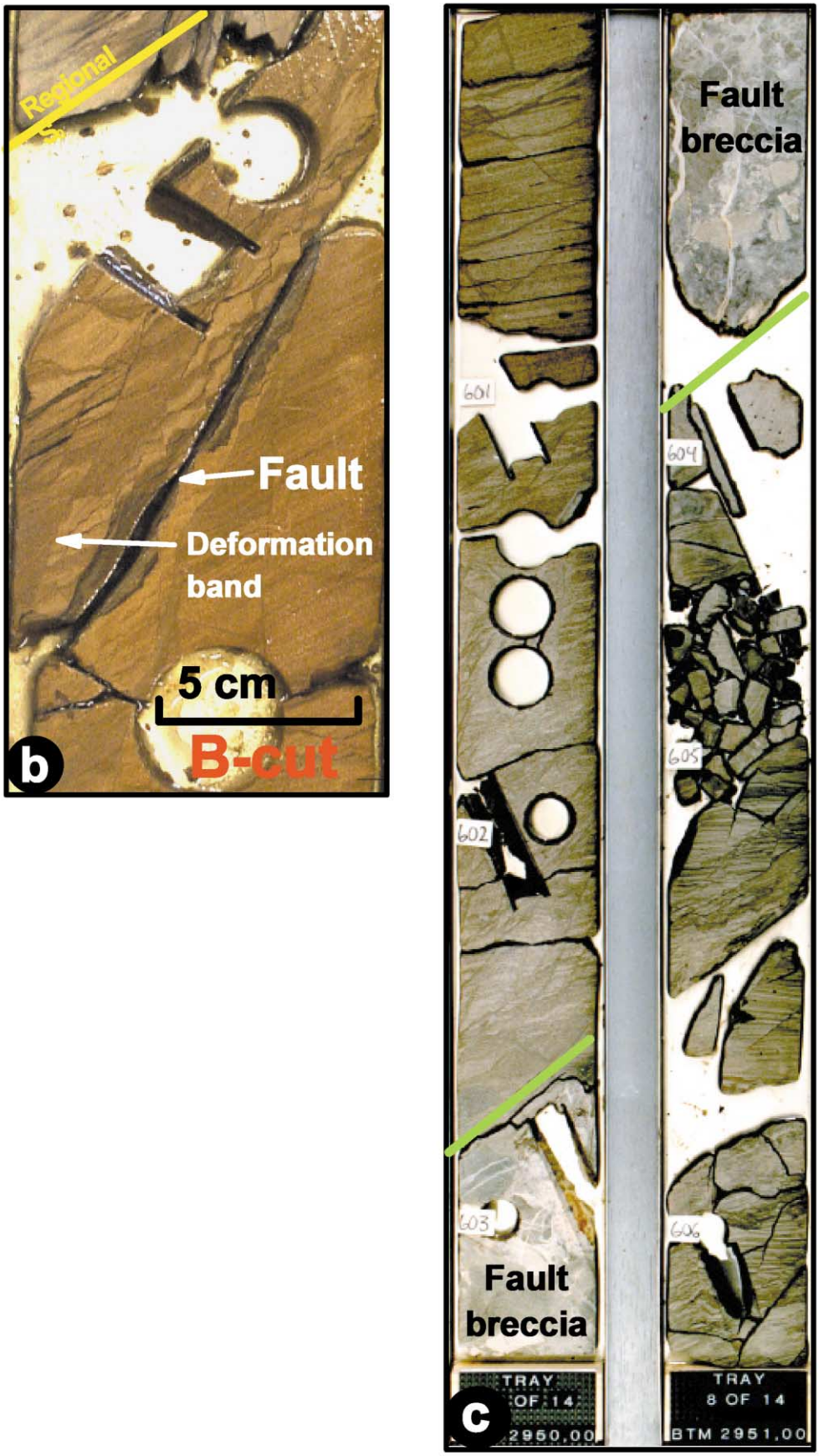

Fig. 4 (*continued*).

of a fault with a discrete slip surface, the deformation bands are commonly characterised by strain hardening due to interlocking of grains and grain crushing. Once a discrete slip surface has developed, further displacement will normally occur along this mechanically weak surface. There is a clear distinction between shear bands and ordinary faults in that shear bands have not developed a discrete slip surface. Slip surfaces occur in shear bands only on the micro scale, where shear cracks may offset grain boundaries, but the length of these surfaces is generally less than a few millimetres.

Fig. 4a shows deformation bands observed in sandstones of the Tarbert Fm. in well 34/10-5, which is a vertical exploration well. Three interconnected deformation bands are apparent. They all touch each other and therefore have a connectivity of two (each deformation band touches two others). The width of the deformation bands varies between 0.5 and 4 mm, and offset varies between 1 and 1.5 cm. The deformation band trace farthest to the right in Fig. 4a is linear, whereas the others are curvilinear. The two curved bands may be a part of an anostomosing system, although the limited core information does not allow this to be determined with certainty. No discrete slip surfaces are associated with the deformation bands shown in Fig. 4a.

Several shear bands are identified within the Ness Fm. in well 34/10-A-15 (Fig. 4b). In addition, a discrete slip surface has developed. The displacement associated with a single shear band is generally less than 1 cm. The total number of shear bands in this interval is less than 100. Thus, the total displacement caused by shear bands must be less than a metre. However, detailed well log correlation shows that the fault zone is associated with a 6 m missing section (Fossen & Hesthammer, 2000). The remaining displacement along the fault must therefore occur along the discrete slip surface that has developed in the central deformation zone. This feature is consistent with observations elsewhere (Fossen & Hesthammer, 1997, 1998b) and suggests that the fault zone displayed in Fig. 4b has reached stage (c) and barely into stage (d) as described above, whereas the shear bands in Fig. 4a reached stage (b).

For larger-scale faults, the deformation zone consists of numerous shear bands, in many cases subparallel to the main fault, and a fault zone of intensely deformed fault rock. The fault zone displayed in Fig. 4c is associated with a breccia formed during movement along the discrete slip planes. Outside this zone, abundant shear bands exist. Detailed well log correlation shows that the fault is associated with 69 m of missing section. This zone of deformation has reached stage (d) as described above, i.e. complex zones of interconnected deformation bands and discrete slip surfaces have developed.

4.2. Deformation mechanisms

In general, shear bands can be grouped into: (1) deformation bands with little or no grain size reduction (i.e. disaggregation structures); (2) deformation bands with grain size reduction (i.e. cataclasis); and (3) shear bands with clay smearing (e.g. Antonellini et al., 1994). The last type can be further separated into a phyllosilicate framework in which the clay smear is discontinuous due to shortage of mica (occurs in mica-rich sandstones), and phyllosilicate smear, in which the clay smears are continuous (occur in

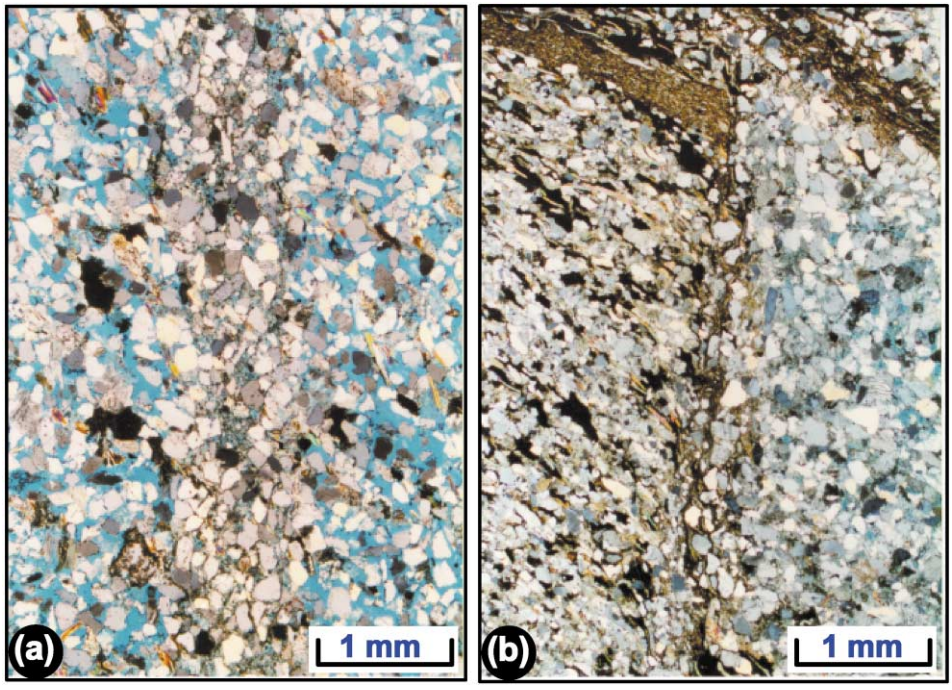

Fig. 5. (a) Microphotograph of a disaggregation structure. (b) Microphotograph of a phyllosilicate framework structure. See text for detailed discussion.

Table 1
Key numbers for amount of drilled and cored reservoir

Formation (Gullfaks)	Drilled reservoir (m)	Drilled reservoir (%)	Cored reservoir (m)	Cored reservoir (%)
All	112 790	100.00	6077	100.00
Heather	6122	5.43	35	0.58
Tarbert	14 781	13.10	1144	18.83
Ness	16 112	14.28	910	14.97
Etive	3869	3.43	314	5.17
Rannoch	13 917	12.34	763	12.56
Drake	11 954	10.60	67	1.10
Cook	17 482	15.50	633	10.42
Amundsen	9881	8.76	188	3.09
Statfjord	7867	6.97	1046	17.21
Lunde	8719	7.73	454	7.47
Others	2086	1.85	523	8.61

Table 2
Summary results from structural analysis of core data

Formation (Gullfaks + Gullfaks Sør)	Def. bands total (number)	Def. bands single (number)	Def. bands Anastom. (number)	Def. bands network (number)	Width (average) (mm)	Displacement (average) (mm)	Hardness (host/fault) (1–5; 5 is hardest)
All	4824	1075	30	3719	1.42	8.61	3.04:3.11
Heather	151	0	0	151	NA	NA	3.00:3.00
Tarbort	669	277	4	388	1.65	11.18	3.02:3.06
Ness	970	180	4	786	1.02	9.24	3.12:3.13
Etive	201	66	0	135	2.21	5.00	2.93:3.13
Rannoch	1624	292	16	1316	1.05	5.43	2.80:2.90
Drake	46	1	0	45	2.51	NA	3.33:3.33
Cook	299	22	0	277	1.02	14.11	3.26:3.07
Amundsen	54	0	0	54	NA	NA	2.71:1.00
Statfjord	679	209	6	464	1.69	8.35	3.27:3.47
Lunde	131	28	0	103	2.13	13.50	3.47:3.56

Table 3
Proportional statistics for shear bands and faults

Faults with more than 5 m displacement within cored intervals	18
Faults (>5 m displacement) per kilometre (from core data)	3.0
Total width of all damage zones (related to faults w/dist. slip surfaces)	478 m (7.8%)
Deformation bands within damage zones (related to faults w/dist. slip surfaces)	3467 (71.9%)
Deformation bands outside damage zones (related to faults w/dist. slip surfaces)	1357 (28.1%)
Non-planar deformation bands	429 (33%)
Planar deformation bands	858 (67%)
Anastomosing bands	30 (0.6%)
Single bands	1075 (22.3%)
Bands within the 168 network zones (connectivity >ca. 5)	3719 (77.1%)
Average connectivity of network zones	22
Average connectivity of single and anostomosing bands	0.6
Connectivity = 0 (single and anastomosing bands)	610 (55.7%)
Connectivity = 1 (single and anastomosing bands)	353 (32.2%)
Connectivity = 2 (single and anastomosing bands)	100 (9.1%)
Connectivity = 3 (single and anastomosing bands)	21 (1.9%)
Connectivity > 3 (single and anastomosing bands)	11 (1.0%)

shales or very impure sandstones; Knipe, 1997; Ottesen et al., 1998).

A common type of shear band in the Gullfaks Field is type (1) where the bands are mostly unaffected by grain crushing and where the material deforms mainly by granular flow (Fig. 5a). Although it is commonly assumed that cataclastic processes are favoured in deeper buried and more consolidated sandstones, we have not seen any indication that the amount of cataclasis increases with depth in the Gullfaks area. This may indicate that depths greater than those of the Statfjord Fm. (650–800 m during deformation) are required for cataclastic processes to become important.

Disaggregation structures in the Gullfaks Field are generally found in sandstones with low phyllosilicate content (less than 20–25%). Deformation bands dominated by cataclasis, i.e. type (2), where a central deformation zone of smaller grains has formed by mechanical fracturing of the original grains, are much less common in the Gullfaks Field. Minor amounts of cataclasis may be related to bands dominated by disaggregation structures or phyllosilicate framework. When the clay content increases beyond 20–25%, the shear bands in the Gullfaks Field are dominated

by phyllosilicate framework (Fig. 5b). Phyllosilicate smear (clay smear) occurs in rocks with a phyllosilicate content of 40–50% or more (Knipe, 1997; Ottesen Ellevset et al., 1998). As such, it may occur in impure sandstone as well as in shale.

Studies from the Gullfaks Field (Q.J. Fisher, R.J. Knipe, D. Condcliffe, and R.M. Jones, personal communication, 1997) show that zones of disaggregation structures are associated with only very minor and negligible decrease in permeability and porosity. Deformation bands with coherent phyllosilicate smears have permeabilities of less than 1 mD and therefore act as efficient seals, whereas the permeability within phyllosilicate framework zones in the Gullfaks Field is generally reduced by two or three orders of magnitude (average of 0.02 mD in the fault rock).

5. Results from individual analyses

5.1. Geometry

A total of 4219 deformation bands from the 6.1 km of cores from the Gullfaks Field and 773 bands from the 2.1 km of cores from the Gullfaks Sør field were analysed (Tables 1–4). The details of all analyses are presented in Hesthammer (1999b) and the reader is referred to that work for more information from the individual wells. The spatial geometry of the deformation structures varies drastically between as well as within individual wells (Fig. 6). Most of the bands (74%) are located within network zones, defined here as zones containing five or more interconnected deformation bands. The average number of deformation bands within a networking zone is

Table 4
Summary statistics for shear bands associated with faults

Well (Gullfaks)	Damage zone from (mMD)	Damage zone to (mMD)	DZ width (m)	Deformation bands in DZ	Missing section (m)
34/10-5	1912	> 1933	21	63	15
34/10-13	1930	1959	29	50	35
34/10-15	2195	2210	15	68	210
34/10-A5H	1848	1853	5	4	6.5
34/10-A5H	1885	1892	7	106	?
34/10-A8	2121	2127	6	238	5
34/10-A14	2281	2286	5	23	10
34/10-A15	2577	2581	4	109	6
34/10-A16	2425	2457	32	236	20
34/10-A21	2763	2782	19	175	45
34/10-B1	2223	> 2285	> 62	> 789	45
34/10-B12	2883	> 2981	> 98	> 393	69 + 92
34/10-B18	4392	> 4395	> 3	> 20	247
34/10-C1	2083	2086	3	84	14
34/10-C3	2363	2442	79	188	9 + 9
34/10-C5	< 3115	3159	> 44	> 272	?
34/10-C14	3650	3673	23	25	8
34/10-C14	< 3543	3563	> 20	> 155	?
34/10-C26	2174	2177	3	56	18
Sum	–	–	> 478	> 3054	863.5

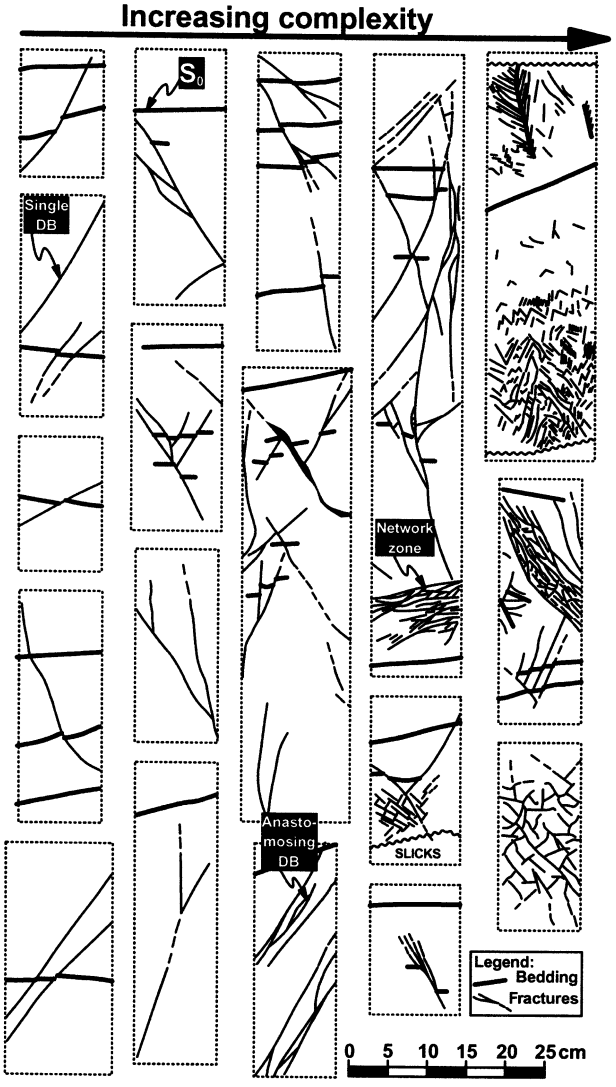

Fig. 6. The shear bands observed in cores from the Gullfaks Field vary drastically both in geometry and density from single planar structures to highly curved bands in complex zones. The figure shows line drawings from a collection of cores from several different wells and deformation zones in the Gullfaks area. For statistical purposes, the shear bands were separated into single, anastomosing and network zones as illustrated in the figure. Bedding dip as observed in the core is shown with thick lines whereas the shear bands are shown with thin lines.

20 (the average width of the zones is 50 cm). 1075 (22%) of the deformation bands are single bands whereas only 30 (0.6%) bands were classified as anastomosing at the scale of observation. Based on observations from the intersection of deformation bands with the slabbed core surface, two-thirds of the bands are planar. The average connectivity (i.e. how many other deformation bands the analysed band intersects) of all single and anastomosing bands is 0.6 and as much as 610 deformation bands did not touch any other bands (i.e. the connectivity is zero). Clearly, since very small portions of the deformation bands can be observed in cores, the true connectivity will be much higher.

5.2. Hardness of host and fault rock

Hardness of shear bands with respect to host rock may be used to indicate which deformation mechanism (cataclasis or disaggregation structures) acted on the rocks. In general, cataclastic deformation bands are harder than the surrounding rocks whereas disaggregation bands have hardness similar to the host rock. However, hardness differences may also be related to later diagenetic alteration. Measurements of hardness of host rock and deformation bands were defined on a scale from 0 (loose sand) to 5 (very consolidated) using a hammer.

For all fractures, the average hardness of the host rock is 3.04, whereas the average fault rock hardness is 3.11 (Tables 1–3 and Fig. 7). Although the difference in hardness is only minor, statistical tests show that, due to the large number of measurements, the difference is significant (the probability for no significant difference based on the *t*-test is only 2%), and is probably related to denser packing and minor crushing of grains within the shear bands. Also, there is no significant differences in hardness between host rock and fault rock for shear bands dominated by phyllosilicate smear, phyllosilicate framework and disaggregation structures, whereas those bands dominated by disaggregation structures and cataclasis or cataclasis alone display significant differences (with a significance level of 5%). Additionally, there is a significant increase in hardness from bands dominated by disaggregation structures to those dominated by cataclasis.

The average hardness of shear bands from the Gullfaks Field is 2.92, whereas the host rock has an average hardness of 2.87 (with a probability of no significant difference of 11%); the average hardness of deformation bands

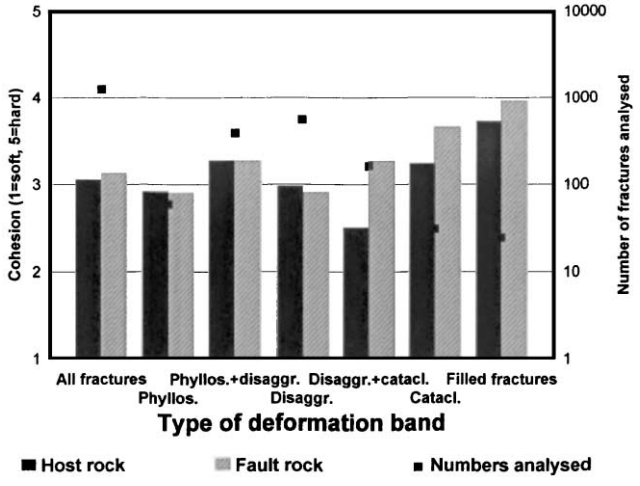

Fig. 7. Plot of hardness of host rock and shear band with respect to type of band. The hardness was measured by simply scratching the rock with a hammer. Loose sand is given a value of 0, whereas the hardest rock is given a value of 5. In general, the fault rock is slightly harder than the host rock, suggesting that minor amounts of cataclasis and grain interlocking are present in the shear zones. See text for explanation.

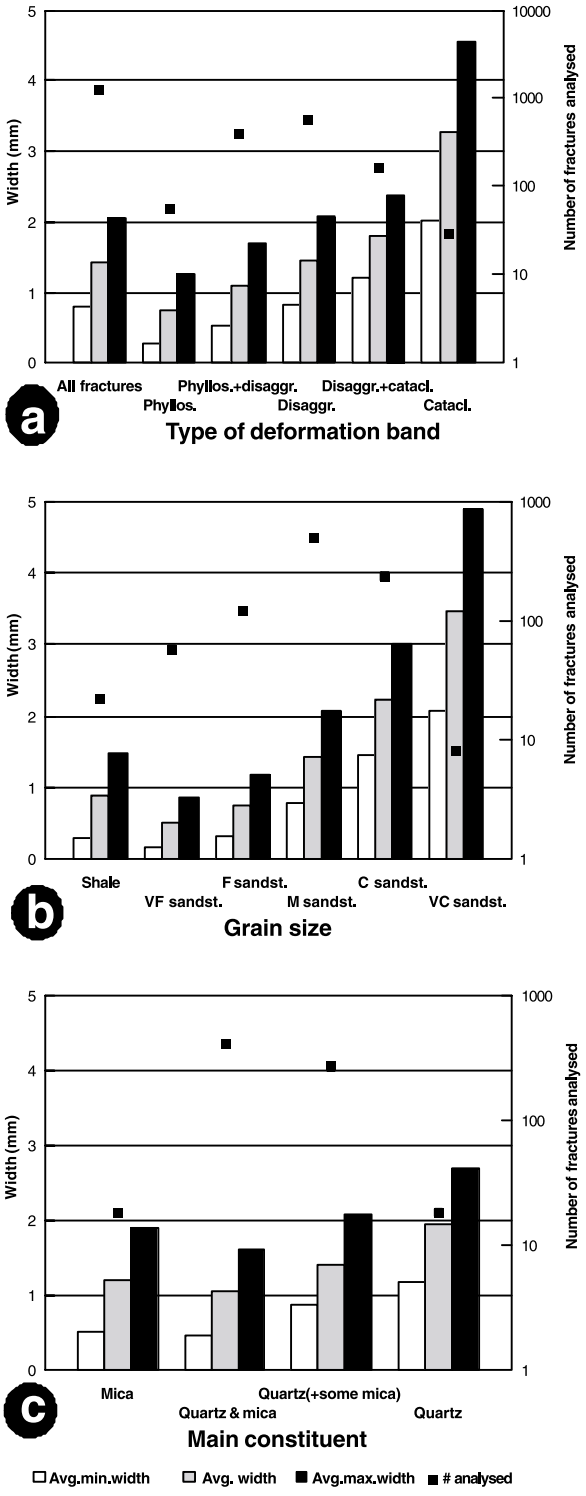

Fig. 8. (a) Plot of width of shear bands with respect to type of band. (b) Same as (a) but for variations in grain size. (c) Same as (a) but for variations in main constituent (mica or quartz; "some mica" refers to less than approximately 30% but more than 10%). The average minimum and maximum widths were obtained by calculating the average of the narrowest and broadest portions, respectively, of each shear band as observed in the core. See text for further explanation.

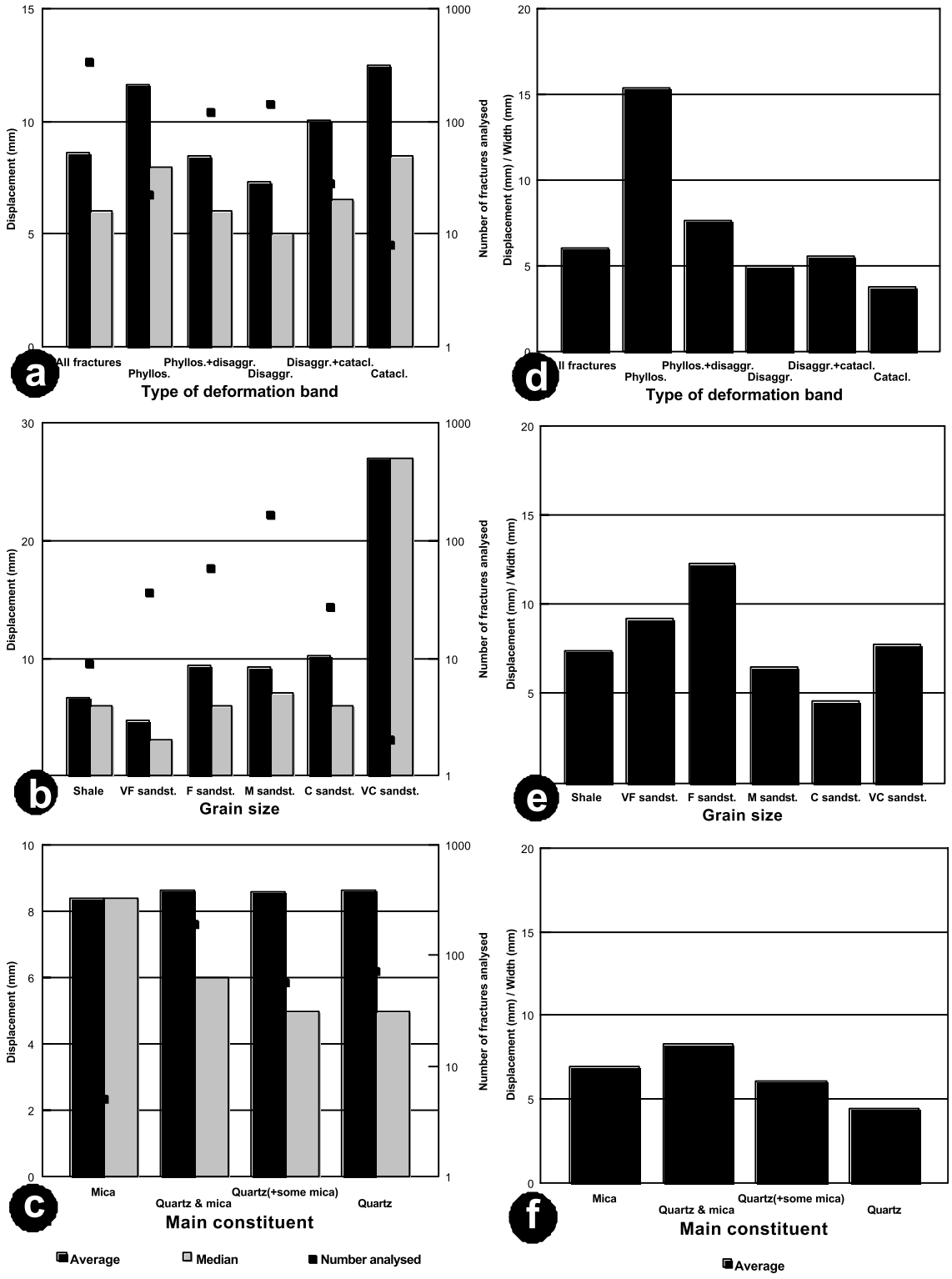

Fig. 9. (a) Plot of displacement of shear bands with respect to type of band. (b) Same as (a) but for variations in grain size. (c) Same as (a) but for variations in main constituent (mica or quartz). (d) Plot of displacement–width ratio with respect to type of band. (e) Same as (d) but for variations in grain size. (f) Same as (d) but for variations in main constituent (mica or quartz). See text for further explanation.

and host rock on Gullfaks Sør is 3.73 and 3.6, respectively (with a probability of no significant difference of only 1%). It is clear from this analysis that both the host rock and shear bands on Gullfaks Sør are more consolidated than on the Gullfaks Field. Although an increase in hardness with depth would be expected on both fields (due to differential compaction prior to deformation), there is no statistical support for this hypothesis. As such, the difference in

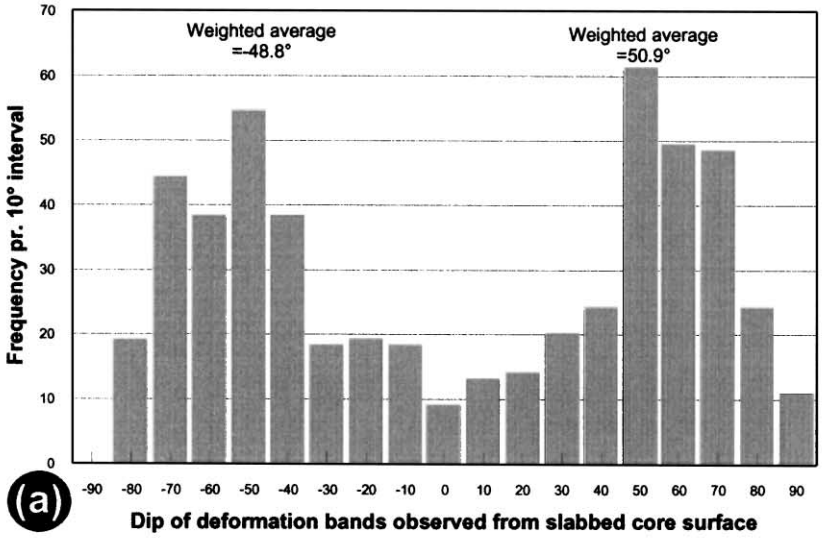
Weighted average
=-48.8°
Weighted average
=50.9°
Frequency pr. 10° interval
0
10
20
30
40
50
60
70
-90 -80 -70 -60 -50 -40 -30 -20 -10 0 10 20 30 40 50 60 70 80 90
(a)
Dip of deformation bands observed from slabbed core surface

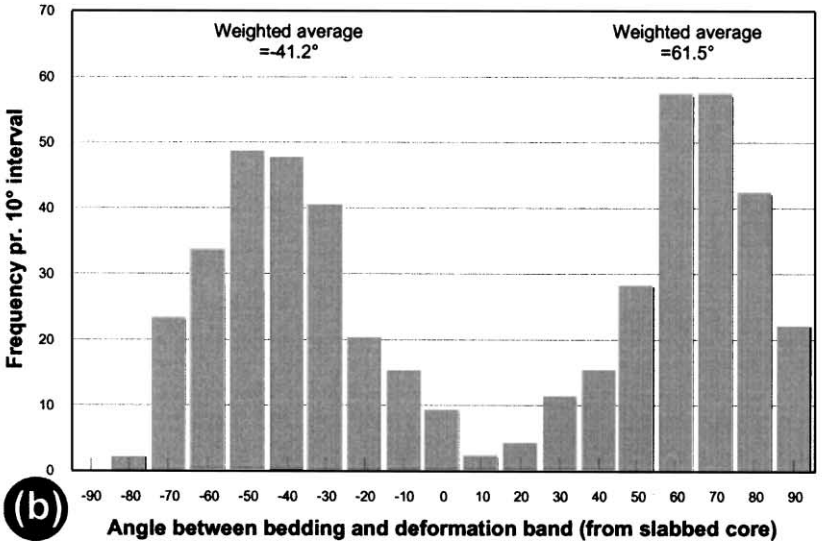
Weighted average
=-41.2°
Weighted average
=61.5°
Frequency pr. 10° interval
0
10
20
30
40
50
60
70
-90 -80 -70 -60 -50 -40 -30 -20 -10 0 10 20 30 40 50 60 70 80 90
(b)
Angle between bedding and deformation band (from slabbed core)

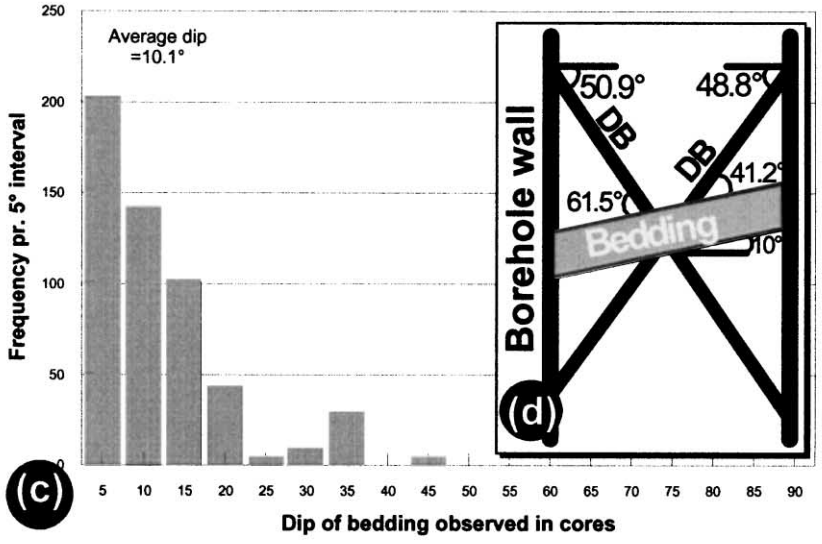
Average dip
=10.1°
Frequency pr. 5° interval
0
50
100
150
200
250
5 10 15 20 25 30 35 40 45 50 55 60 65 70 75 80 85 90
(c)
Dip of bedding observed in cores
Borehole wall
50.9°
48.8°
DB
DB
61.5°
41.2°
Bedding
10°
(d)

Fig. 10.

deformation band hardness between the Gullfaks Field and Gullfaks Sør is likely related to a higher degree of post-deformational lithification and enhanced quartz precipitation within the shear bands on Gullfaks Sør due to elevated reservoir temperatures (above 120°) and enhanced fluid flow along the shear bands. The differences in shear band characteristics between the Gullfaks Field and Gullfaks Sør demonstrate that data cannot be uncritically extrapolated from one field to another even if they are geographically close unless the controls on processes affecting flow of hydrocarbons are understood.

5.3. Width of shear bands

Studies of the width of individual shear bands with respect to type, grain size and main constituent show clear and very interesting relationships (Fig. 8). The average width of single bands is 1.42 mm, but shows a significant increase from 0.75 mm for fault rocks dominated by phyllosilicate smear or framework to 3.28 mm for those dominated by cataclasis (Fig. 8a). A similar relationship exists for the width of deformation bands in sandstones with respect to grain size. Here, the average width increases from 0.51 mm within very fine-grained sandstone, to 3.47 mm for very coarse-grained sandstone (Fig. 8b). The average width of the shear bands increases from 1.04 mm in rocks with equal amounts of quartz and mica as main constituents, to 1.95 mm for bands in rocks containing mainly quartz (Fig. 8c). This is probably because the presence of mica constrains the localised deformation to narrower zones than for microfaults within coarser and cleaner sandstones.

A notable observation from Fig. 8b and c is that shear bands in rocks with high shale content are somewhat wider than those in fine-grained sandstones. Also, there is no clear relationship between the width of the shear bands and the depth at the time of deformation (the Brent Group was near the surface when deformation started whereas the Statfjord Fm. was buried to approximately 650–800 m depth).

5.4. Apparent displacement associated with shear bands

Fig. 9a–c shows plots of average and median observed displacement versus type, grain size and main constituent. It is commonly not possible to observe the displacement related to a single band in homogeneous sandstones. However, the presence of phyllosilicate laminae aids the displacement analysis. The average observed displacement for all the shear bands is 8.61 mm (6.00 mm for median displacement). However, this measurement is misleading for at least two reasons. First, the displacement is measured from the slabbed core section. This section is commonly oblique to the shear band and the observed (apparent) displacement is therefore generally larger than the true displacement. This uncertainty can be compensated for by finding the true orientation of the shear bands (Hesthammer & Henden, 2000a). Second, the maximum displacement that can be measured is restricted by the limited width of the core (typically 6–10 cm), causing an under-representation of large displacement values. There is no significant relationship between displacement and type of shear band, grain size or mineralogy. Nor has any relationship between displacement along microfaults and depth at the time of deformation been detected.

Fig. 9d–f shows displacement–width ratio versus type, grain size and main constituent. Fig. 9d indicates that deformation bands dominated by phyllosilicate smear or framework are thinner and with larger displacement than the deformation bands in cleaner sandstone dominated by disaggregation structures or cataclasis. This finding suggests that the presence of phyllosilicates helps localise the shear deformation and reduces the internal friction within the bands. There is no clear relationship between the displacement–width ratio and grain size. Fig. 9f supports the findings in Fig. 9d in that the deformation bands in clean quartzose sandstones have the lowest displacement–width ratios.

5.5. Angle between bedding and deformation bands

An important, but commonly neglected type of information that can be obtained from structural core analysis is the orientation of microfaults with respect to borehole wall and bedding. Since most cores are unoriented, the trace of a fracture on the slabbed core surface from a vertical well only reflects apparent rather than true dip. However, the fact that the true dip can only be equal to or steeper than the apparent dip may be useful. In addition, shear bands in the Gullfaks area are generally associated with larger-scale faults with several metres displacement and discrete slip surfaces. Diagenetic and mineralogical studies (Q.J. Fisher, R.J. Knipe, D. Condcliffe, and R.M. Jones, personal communication, 1997) suggest that most shear bands formed at shallow burial depths, likely associated with the main extensional event that started immediately after deposition of the Brent Group. Dipmeter analyses demonstrate that more than 60% of the faults in the Gullfaks Field are associated with the local drag of the bedding (Hesthammer & Fossen, 1998). This means that the bedding is rotated towards parallelism with the fault. Thus, when the fault is cored, the shear bands strike roughly in the same direction

Fig. 10. (a) The dip of shear bands as observed in subvertical wells is approximately 50° both for those bands dipping in the same direction as bedding and those oriented antithetic to bedding. (b) When the angle between bedding and shear bands are plotted, an asymmetry is observed. The angle between bedding and shear bands dipping synthetic to bedding is smaller than those dipping opposite of bedding. (c) The average dip of bedding in the subvertical wells is 10.1°. (d) The data seen in diagrams (a)–(c) suggest that bedding rotation took place prior to the development of shear bands and that no rotation occurred after faulting.

as the bedding. This model can actually be controlled by investigating the intersection of the shear band with the section oriented perpendicular to the slabbed core surface. Since the core is slabbed to display the highest dip of bedding, both the bedding and shear band intersections should be oriented perpendicular to the borehole wall. By using this criterion, it is also possible to eliminate from the analysis all microfaults that do not strike parallel to the bedding.

Fig. 10a shows a frequency distribution diagram based on orientation analyses of shear bands from all (29) wells on the Gullfaks Field and Gullfaks Sør that are deviated less than 10° from vertical (i.e. subvertical wells). Dip along the *x*-axis is plotted from −90 (shear bands are oriented synthetic to the bedding dip) to +90° (shear bands dip opposite of bedding). Since the wells are subvertical, the apparent dip of the bands will be close to, but somewhat less than, the true dip (assuming that most bands strike subparallel to the bedding). The data define a straight line in log–log space (plotting the cumulative number against dip of deformation bands), indicating that the data are parametric and follow a Gaussian (normal) distribution. The weighted average dip is 48.8° for shear bands oriented synthetic to the bedding, and 50.9° for shear bands antithetic to the bedding. The simplest explanation for this observation is that the shear bands constitute a conjugate system where each set dips approximately 50° or more. The symmetry further indicates that the 50° dip also reflects the minimum initial dip (later rotation would have imposed a difference in angle). Since only a few of the total number of fault zones on the Gullfaks and Gullfaks Sør fields are included in the diagrams shown in Fig. 10, the results should be treated with care. For instance, most of the 18 cored faults with displacement larger than a few metres on the Gullfaks Field are minor faults (less than 100 m displacement), and it is uncertain to what extent these results reflect the deformation associated with the main faults in the field.

An interesting asymmetry is observed when the dip of the shear bands is plotted relative to bedding (Fig. 10b). Here, the weighted average angle between the bedding and shear bands dipping in the same direction as the bedding is calculated to 41.2°, whereas the weighted average for bands dipping opposite of the bedding is 61.5°. The average dip of the bedding is 10.1° (Fig. 10c). The relationships between the different observed angles are shown in Fig. 10d. The simplest explanation for the observed asymmetry is that the bedding was slightly rotated prior to the development of the shear bands. If this observation is general for the area (which it may not be), it suggests that most of the small-scale block-internal faulting on the Gullfaks Field postdates the rotation of the bedding. Also, since both sets of shear bands have very similar (48.8 versus 50.9°) "true" dips, very little rotation took place after the development of the related minor faults. We emphasise that the geometric relationship between the shear bands and bedding presented here (Fig. 10) is restricted to mostly minor faults in the field. Major (domino) faults are generally not cored in the area, and the same relationship is unlikely to hold for their associated shear bands (damage zones). This implies that most minor faults in Gullfaks formed at a late stage in the extensional phase, probably due to compatibility problems during movements along the main faults (Fig. 1).

5.6. Fracture distribution

Several studies suggest that fracture density and distribution is a function of burial depth and degree of consolidation, lithology, grain size, bed thickness, distance to major faults, local stress patterns, sampling effects and displacement (Aarland & Skjerven, 1998; Gabrielsen & Aarland, 1990, 1995; Gabrielsen & Koestler, 1987; Harris et al., 1960; Huang & Angelier, 1989; Ladeira & Price, 1981).

Fracture frequency diagrams are useful for the evaluation of the spatial distribution of fractures. Fig. 11 shows such diagrams for eight wells on the Gullfaks Field that have penetrated faults with several metres displacement. Fracture frequency is plotted along the *y*-axis and measured depth in the well along the *x*-axis. Ideally, the *x*-axis should reflect distance perpendicular to the fault rather than along the wellbore path in order to exhibit the true thickness of the damage zone (i.e. the zone around the fault that contains deformation bands; see below). Correcting for this difference would require knowledge of the orientation of the faults. However, most faults on the Gullfaks Field with displacement less than 30 m cannot be identified from seismic data due to limits in seismic resolution (Hesthammer & Henden, 2000b), and it is therefore not possible to accurately identify the orientation of the faults. As a result, the true thickness of the damage zone will be somewhat less than that observed along the wellbore path (displayed in Fig. 11).

All faults with several metres displacement or more on the Gullfaks Field are associated with a narrow deformation zone with abundant shear bands or deformation bands. The width of the zone seldom exceeds a few tens of metres. There is no obvious relationship between the missing section associated with fault displacement and the width of the damage zone (Fig. 12a), although a broad distinction may possibly (but with large uncertainties) be made between faults associated with missing section less than 15–20 m (the width of the deformation zone is mostly less than 20 m) and those with missing section above 15–20 m (the width of the damage zone exceeds 20 m). However, this distinction is dependent on whether the observed damage zone is associated with a single fault surface or several minor fault structures (this uncertainty is indicated in Fig. 12a). Commonly, the cored sections are discontinuous, and could therefore possibly contain several smaller slip surfaces within missing sections (discussed in detail by Fossen & Hesthammer, 2000).

Whereas core data demonstrate the presence of a narrow

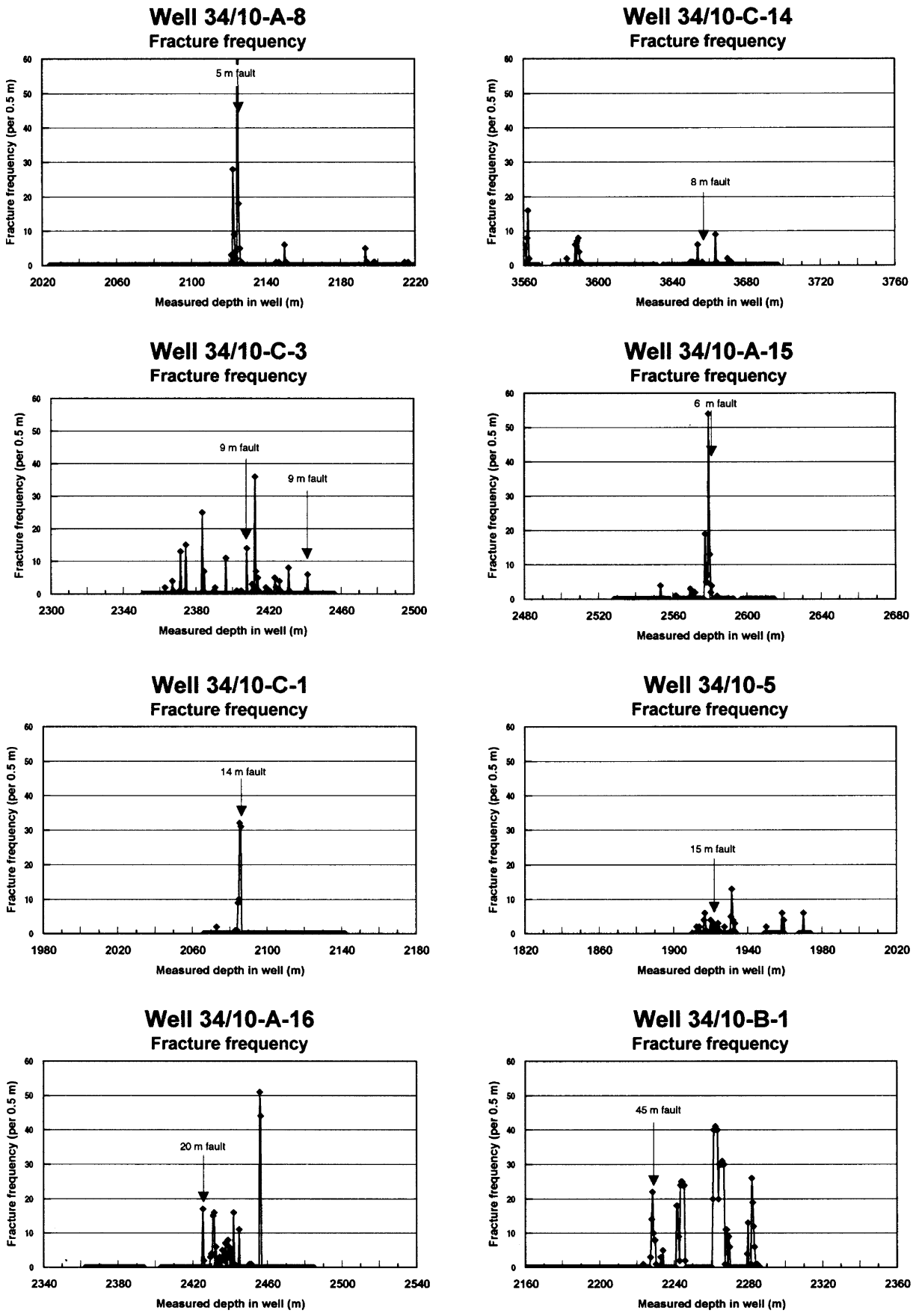

Fig. 11. Fracture frequency (per 0.5 m) diagrams for eight wells containing core data from faults with several metre displacement. All faults are associated with a narrow damage zone containing abundant shear bands.

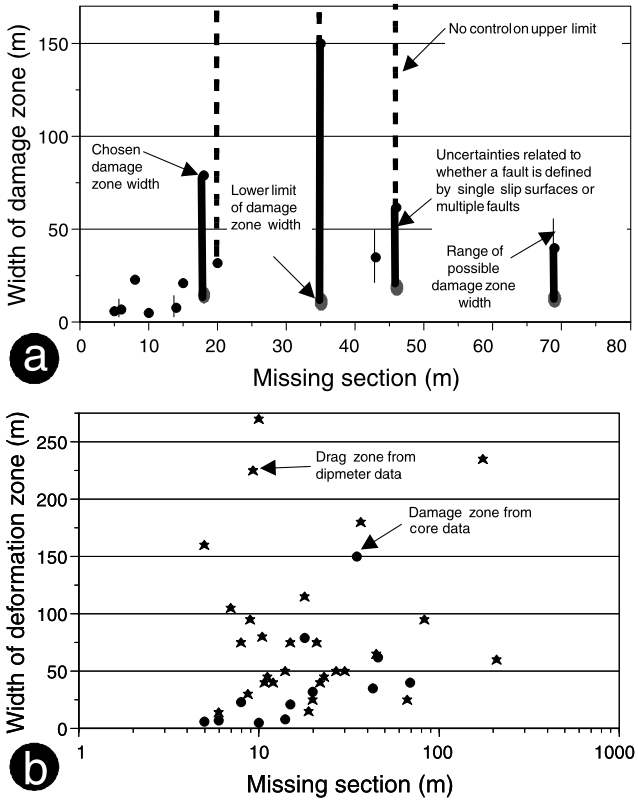

Fig. 12. (a) Plot of missing section against the width of the damage zone to faults. Since there exist uncertainties related to whether or not a damage zone contains one or more distinct slip surfaces, it was necessary to define a range of damage zone widths for some of the faults (indicated with arrows). There is no obvious linear relationship between the width of the damage zone and the amount of missing section associated with the fault. However, there appears to be a broad division between faults larger than 20 m (damage zone is 15–80 m wide) and faults associated with less than 20 m missing section (damage zone <20 m wide). (b) Comparison of the width of damage zones as observed from core data (filled circles) and drag zones as observed from dipmeter data (filled stars). The drag zones are on average wider than the damage zones, indicating that much of the deformation was by a mechanism other than discrete faulting.

damage zone with numerous shear bands, dipmeter data reveal that most faults in the Gullfaks area are also associated with a deflection of bedding (termed local drag; Hesthammer & Fossen, 1998). A comparison of the width of the damage zones and drag zones show that, on average, the drag zones are wider than the damage zones (Fig. 12b). This suggests that some of the deformation must have been by a mechanism other than discrete faulting, an observation that will influence models for fault zone development.

The lack of obvious correlation between the damage zone width and displacement is probably related to the evolution of faults from shear bands. Shear bands (generally considered as zones of strain hardening) typically form prior to the development of a fault with distinct slip surface (Aydin & Johnson, 1978, 1983). Once a discrete slip surface has developed, further displacement will normally occur along this weak surface. Fig. 13 shows a fracture frequency diagram for well 34/10-A-19 on the Gullfaks Field. Although a zone with abundant deformation bands is observed around 2025 mMD (metres measured depth), no section is missing as indicated from the detailed well log correlation. Furthermore, the cored section is continuous and excludes the possibility for location of a fault with several metres displacement within this damage zone. It is likely that the cluster (network) zone observed around 2025 mMD in well 34/10-A-19 represents stage (c) as described earlier, where a complex zone of interconnected deformation bands has formed, and that stage (d) has not been reached (i.e. no discrete slip surface or fault exists). As such, the damage zone width simply reflects the amount of strain accommodated prior to localisation along a slip plane.

5.7. Variations in bedding orientation

A useful parameter to record together with fracture frequency is changes in the bedding dip as observed in the core. Although such measurements will not yield exact information on changes in the true bedding orientation, the relative changes in the dip will help to identify zones of rapid or gradual changes that may be caused by steepening or flattening drag associated with faulting (Bengtson, 1981; Hesthammer, 1998). Fig. 14a shows a fracture frequency diagram for well 34/10-B-1. The upper part of the well is located in the hanging wall to one of the main faults within the domino system on the Gullfaks Field. A fault associated with a 45 m missing section is identified at 2232 mMD. The fracture frequency diagram shows that there is very little deformation in the hanging wall to this fault (i.e. above 2232 mMD). In the footwall, however, a 60 m wide damage zone is developed. This is likely related to a main, seismically observable, east-dipping fault with a 167 m missing section (identified from well log correlation) located at 2332 mMD. A plot of changes in the dip of bedding (as observed in the core; i.e. the observed bedding dip does not represent true dip) against measured depth in the well (Fig. 14b) shows that the dip of bedding is fairly constant, or slightly decreasing, in the interval above the 45 m fault. Below this, the bedding dip increases drastically from 25 to 50° (apparent dip in core). Since the bedding dip increases towards the main fault located at 2332 mMD, the fault must be associated with steepening drag. The dip direction of the fault can be determined by identifying the dip direction of the bedding within the area affected by the drag.

Dipmeter data from the well (Fig. 14c) are highly scattered in the interval between the 45 m fault located at 2232 mMD and the 167 m fault located at 2332 mMD. However, there appears to be a general increase in dip from subhorizontal at 2210 mMD (a false average of approximately 5° is expected due to the plot type; Hesthammer & Fossen, 1998) to 35° at 2320 mMD. The azimuth versus depth plot shows that the bedding in this interval dips mostly to the east, whereas the general dip of bedding

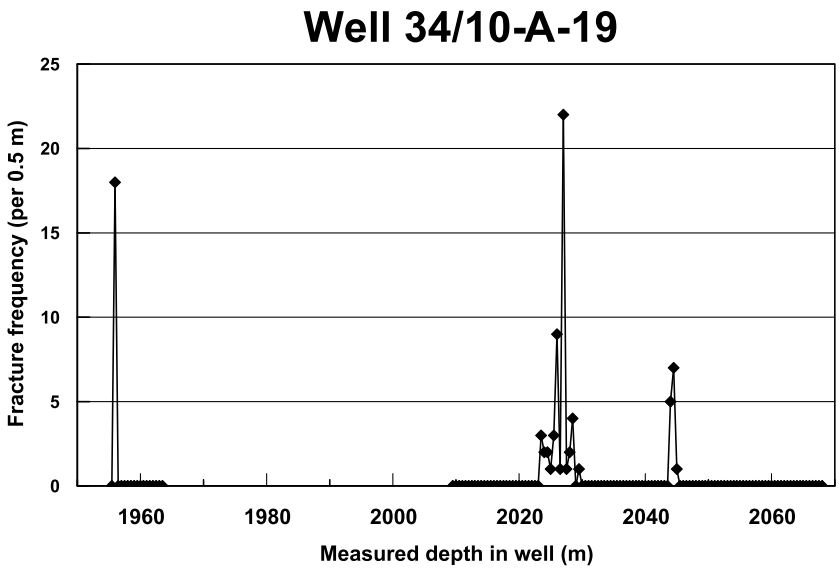

Fig. 13. Fracture frequency (per 0.5 m) diagram for well 34/10-A-19. Although no faults have been identified from detailed well log correlation, a cluster zone of abundant shear bands exists. This suggests that the zone has not reached the stage where a fault with discrete slip surface has developed.

outside the faulted zone is to the west. The observed steepening drag between the two faults observed both in core data (Fig. 14b) and dipmeter data (Fig. 14c) is consistent with drag in the hanging wall to a main east-dipping fault (as identified from seismic data; Fig. 14d). The maximum dip of bedding observed from the dipmeter data is 35°, suggesting that the main fault must have an equal or steeper dip (seismic data indicate a dip of 30–40°). The example from the well 34/10-B-1 demonstrates how the integrated use of seismic data, well log correlation data, dipmeter data and core data can be used to constrain the structural geology of an area.

5.8. Fracture orientation

While oriented core data provide the geologist with information on bedding and fault orientation (e.g. Aarland & Skjerven, 1998), it is often assumed that orientation data cannot be obtained from unoriented cores unless the core can be calibrated against image data such as FMS or FMI. This is not the case. One approach is to orient the core by analysing remanent magnetism in a core sample and compare that with the present magnetic field (Rolph, Shaw, Harper, & Hagan, 1995). Also, there is a simple relationship between observed bedding from core data, the well orientation and true bedding orientation. This relationship can be expressed by a simple formula that will give a solution population for possible bedding orientations as observed from the unoriented cores (Hesthammer, 1998). A similar relationship exists between true bedding orientation, well orientation and the intersection of a surface, such as a fault, with a slabbed section of the core (as is typical for core photographs). Similar to obtaining a solution population for possible bedding orientations, a solution population diagram may be generated for possible fault orientations using simple vector calculations and polar co-ordinates (Hesthammer & Henden, 2000a). The use of stereographic projection simplifies the procedure by avoiding the use of mathematics and may be the preferred method if only a few measurements are to be oriented (Hesthammer, 1999b).

Results from orientation analyses of deformation bands from the Gullfaks area show that bands within the fault zone tend to be subparallel to the distinct slip surface. Within the damage zone, preliminary results indicate that shear bands associated with minor faults (less than 20 m displacement) are subparallel to the main slip surface whereas more than one set of bands exists in damage zones to larger faults (more than 20 m displacement). The strike of the sets is generally subparallel to that of the main slip surface. This difference may be related to changes in the geometry of the main slip surface as the displacement increases, either because the fault crosses different lithologies or because smaller faults join into a larger structure (see Hesthammer, Johansen, & Watts, 2000, for more details on this topic).

6. Discussion of results in view of other data and models for reservoir performance

6.1. Comparison with seismic data

All seismic data contain a mixture of signal and noise and the interpreter is challenged to separate real features from those that are caused by noise interference patterns. This represents a problem on the Gullfaks Field when interpreting seismic attribute maps such as the timedip map, which contains numerous (curvi-)linear features that look very

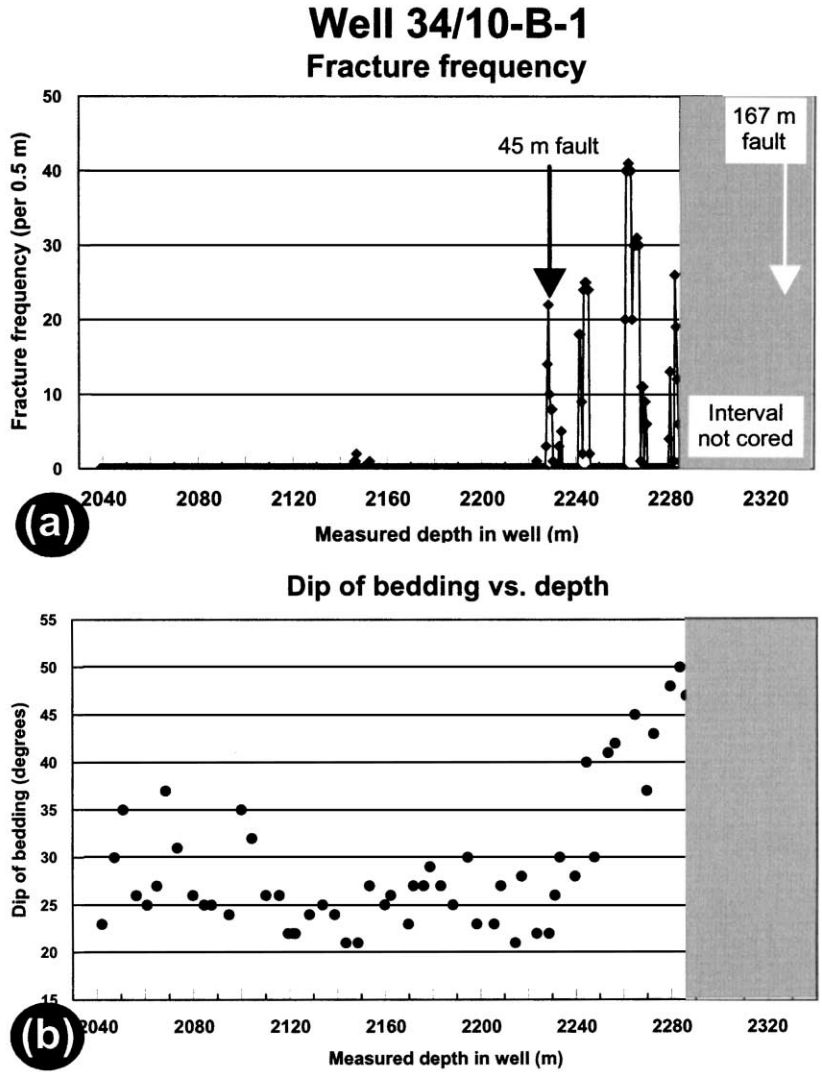

Fig. 14. (a) Fracture frequency (per 0.5 m) diagram from well 34/10-B-1. (b) Dip of bedding (as observed in the core) versus measured depth. (c) Dip versus depth and dip direction versus depth plots for the well. See text for discussion. (d) Geological profile along well 34/10-B-1 based on seismic interpretation and well data.

similar to those generated by faults (Fig. 15). In the early stages of seismic attribute mapping on the Gullfaks Field, it was believed that all of the (curvi-)linear features represented faults. However, integrated studies of dipmeter data, well log correlation data and reflection seismic data have since shown that many of the (curvi-)linear features are related to the interference of dipping coherent noise with real reflections (Hesthammer, 1998, 1999a,b; Hesthammer & Fossen, 1997a,b, 1998; Hesthammer & Løkkebø, 1997). The seismic noise causes the real reflections to break up and rotate in the direction of the dipping noise, thus giving the appearance of faults with up to 30 m displacement (Hesthammer, 1999a). Statistics from structural core analyses carried out on the Gullfaks Field can be used to further support the conclusions based on analyses of dipmeter data and well log correlation data.

A total of 18 faults with associated missing section ranging from 6.5 to 247 m have been identified from detailed analyses of 6.077 km of core data from the main Gullfaks Field. This gives a frequency of 3.0/km for faults with missing section larger than 6 m. However, the sampling is not entirely random. Most wells are either drilled as injectors located close to block-bounding faults in a hanging wall position, or as producers located at the crest of the rotated fault blocks. The frequency of faults encountered in the wells is also dependent on the well orientation. Analyses show that, when projected into the horizontal plane, there is no dominant drilling orientation, i.e. the horizontal E–W component of available core data is more or less equal to the N–S component (1.6 vs. 1.9 km).

The fault frequency observed in the core data may be compared to the frequency of (curvi-)linear features on seismic attribute maps to indicate whether or not the features are

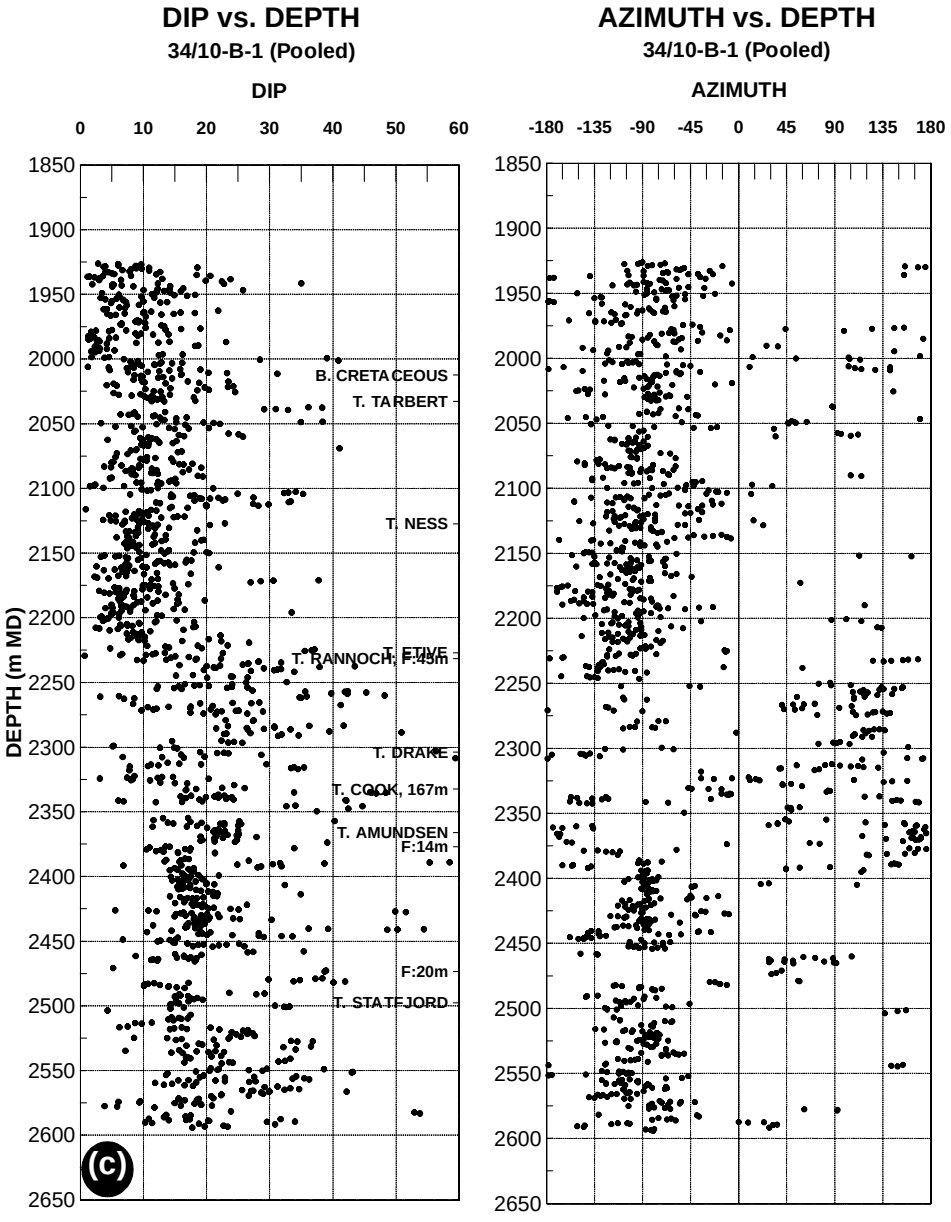

Fig. 14 *(continued).*

noise-related. The average density in E–W direction of west-dipping (curvi-)linear features associated with westerly dip observed on seismic timedip maps from the intra-Ness Fm. reflection on the Gullfaks Field is approximately 9/km (Fig. 15). The length of the cores when projected perpendicular to structures dipping 30° to the west (i.e. perpendicular to the features causing the curvilinear features) is 3.8 km. This gives a fault frequency (where each shear band cluster zone is counted as one fault) of 3.2/km (12 faults with less than 30 m displacement divided by 3.8 km of core data oriented perpendicular to a plane dipping 30° towards 270), much too low to explain all the (curvi-)linear features observed on the seismic attribute map as being caused by faulting.

The well data clearly demonstrate the presence of subseismic faults in the Gullfaks Field. From core analyses, 21 likely locations of faults were mapped based on the presence of distinct damage zones, including all 18 faults identified from well log correlation (Tables 1–4). This indicates that approximately 85% of the faults are detectable by reservoir zonation correlation with other wells. Analyses of dipmeter data indicate a fault frequency of 2.7/km (Hesthammer & Fossen, 1998), whereas detailed well log correlation from all wells in the Gullfaks Field shows a fault frequency of 1.9/km (247 faults within 128.4 km of drilled reservoir). Based on well log correlation data, the frequency of faults associated with less than 30 m missing section is 1.2/km (Fig. 16a). Efforts to identify faults penetrated by

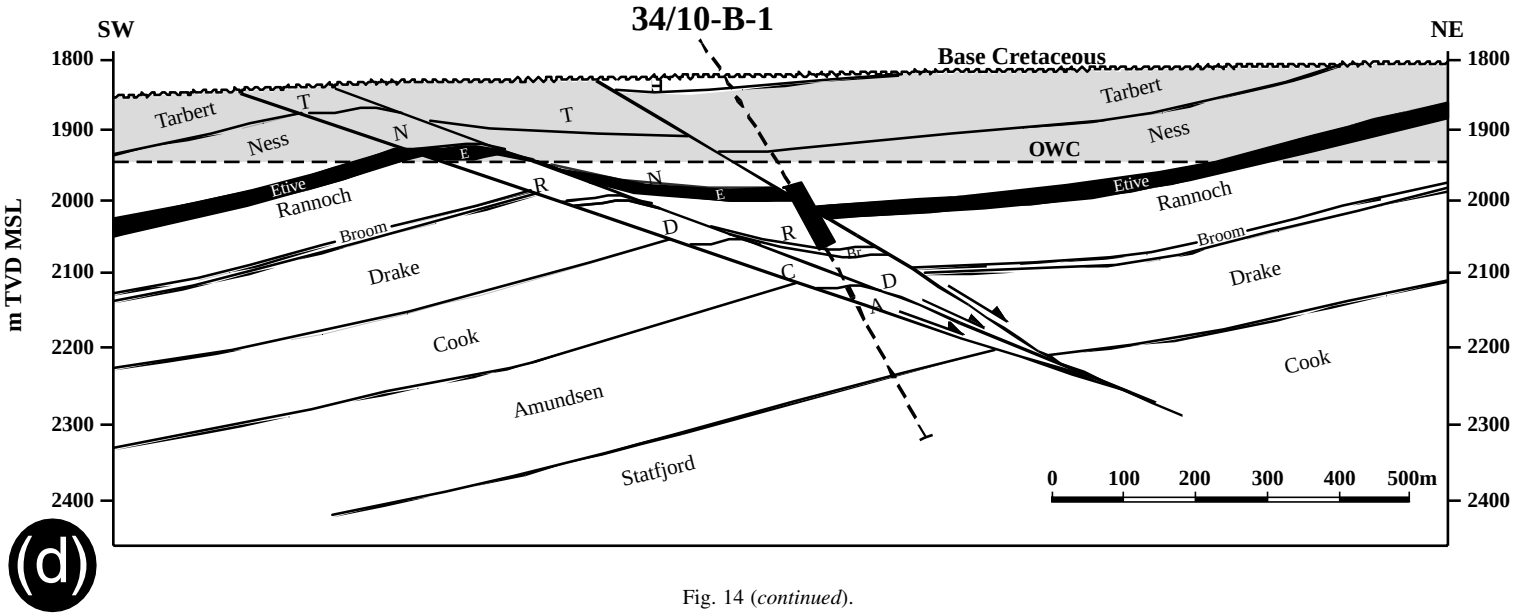

Fig. 14 (*continued*).

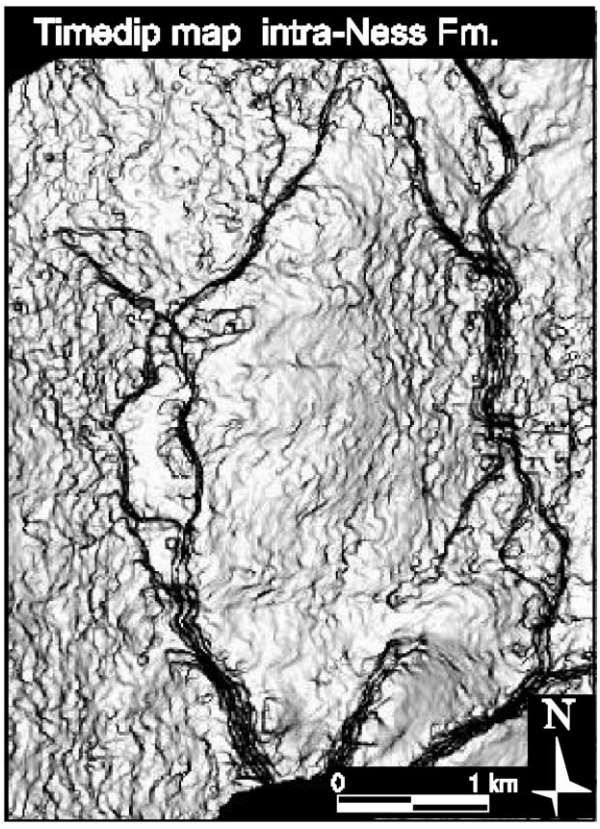

Fig. 15. Timedip map of the intra-Ness Fm. reflection from parts of the Gullfaks Field. The abundant (curvi-)linear features are caused by the interference of dipping coherent noise with real reflections. This interference causes the reflections to break up and rotate in the direction of the dipping noise, thus causing apparent fault offsets in the order of 5–35 m. See Hesthammer (1999a,b) for further explanation of the interference patterns.

wells on seismic data show that, for faults associated with less than 30 m missing section, only 24% can be observed (Fig. 16b). For faults with missing section larger than 30 m, most can be observed in the seismic data, indicating that the practical seismic resolution occurs for faults with approximately 30 m displacement. The expected average frequencies of faults that can be observed in seismic data from the Gullfaks Field are found by multiplying fault frequency from well log correlation (Fig. 16a) with the percentage of faults identified in seismic data (Fig. 16b). The results are shown in Fig. 16c and provide useful input to the number of faults with varying displacement that can be observed in seismic data.

Based on the analyses above, only three of the 12 faults associated with less than 30 m missing section observed from core data can be expected to be observed in the seismic data. This gives a fault density of only 0.5/km (0.8/km when the core data are projected perpendicular to the west-dipping noise features observed on the seismic attribute maps) and strongly suggests that most of the features observed in the seismic data are caused by noise interference rather than actual faulting (see also Hesthammer & Fossen, 1997a).

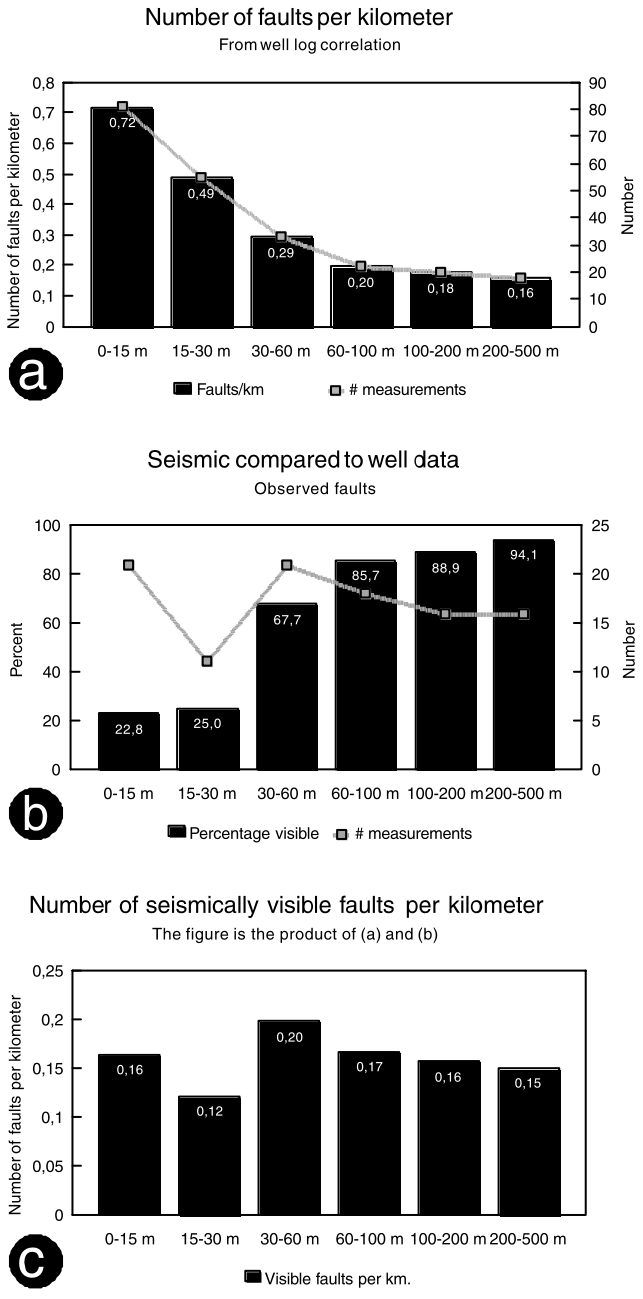

Fig. 16. (a) Number of faults per kilometre as identified from detailed well log correlation. (b) Percentage of visible faults in seismic data (i.e. identified after the well is drilled and the existence of a fault is documented) as a function of displacement. Restrictions in seismic resolution cause most faults with displacement less than 30 m to be invisible in the seismic data. (c) Frequency of seismically observable faults based on observations from well log correlation and seismic data. The diagram is simply the product of the results shown in (a) with the results shown in (b).

6.2. Fault statistics

The apparent displacements encountered in the cored section are plotted in Fig. 17. They show a non-linear trend that is not compatible with a linear or a power-law curve. This may be expected, since only a small subset (392)

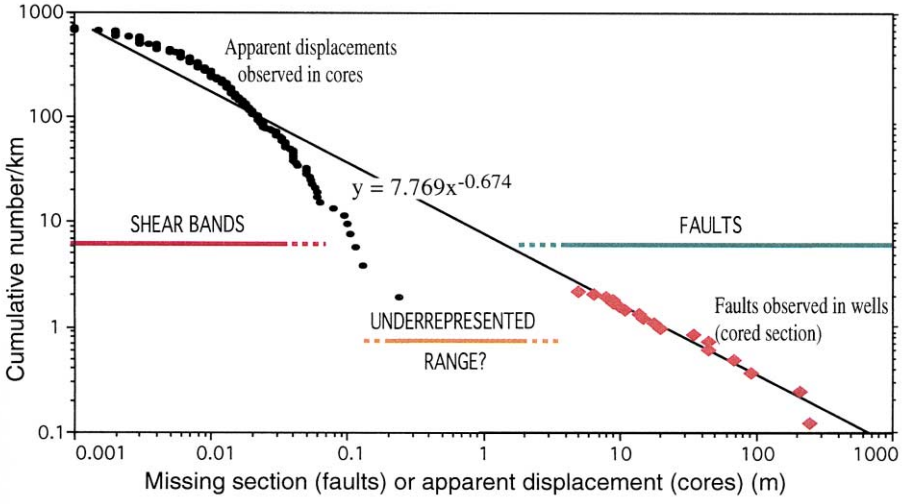

Fig. 17. Cumulative frequency plot of missing section for faults and deformation bands from the Gullfaks Field. The fault data were detected through careful well-log correlation, whereas the shear band data are collected from detailed core analysis. See text for detailed discussion.

of the entire shear band population have measurable displacement in the cores, and since small displacements are favoured in the data sets for reasons discussed above. The fact that they are apparent rather than true displacements also has some influence on the distribution of displacement, although the effect is likely to be small in log–log diagrams.

Faults in the cored intervals that are detected by the sedimentologists through detailed well-log correlation and verified during the core study are also shown in Fig. 17. The 18 faults define a straight power-law line in Fig. 17, with a gradient of −0.674.

When the trend of the well-log correlation data (correlation line) is extrapolated into the size-range of shear bands (core observations), it appears that the core data fit the line reasonably well. A popular conclusion would be that the displacement distribution is fractal from the 100-m scale down to the millimetre scale — a conclusion which indeed has been drawn for other, similar datasets (e.g. Needham, Yielding, & Fox, 1996). This model predicts a large number of hidden faults in the large gap between the two data sets. However, we were only able to recognise 21 faults during core examination (with range in missing section from 247 to 6.5 m, i.e. about 2 orders of magnitude), only three were too small to be detected during well log correlation, and thus <9–6.5 m (resolution of the well-log correlation method in the area). In contrast, the number of faults predicted by the power-law relationship outlined above (extrapolated line in Fig. 17) is about 170 faults in the offset range of 20 cm to 6.5 m. Hence, a significant data gap appears to exist for this range. Uncertainties are involved in this reasoning, such as the presence of rubble zones in the cored section and possible failure to recognise faults in deformation band swarms and large displacement on individual shear bands. These uncertainties are discussed in detail in Fossen and Hesthammer (2000). If our assumption is true, it means that communication may be better than expected in these reservoirs.

6.3. Implications for fault zone development

An idealised, mature fault zone in the Gullfaks Field consists of: (1) a zone of ductile deformation where bedding is deflected along the fault (commonly referred to by the somewhat misleading term “drag zone”, erroneously implying that its formation is related to friction-controlled deformation during fault slippage); (2) a zone of shear bands or microfaults (damage zone); and (3) a discrete slip surface and the associated fault zone. In simple terms, it may be proposed that the numbering above corresponds to their relative time of formation within a single deformation zone (Fig. 18). Ductile bending of the layers is less likely once a weak fault surface has formed unless a complex geometry of the fault plane favours further development of the “drag” zone. Similarly, deformation band formation involve strain hardening processes in many cases, and are generally abandoned once a neighbouring weak slip plane forms.

As demonstrated in Fig. 12b, there are not enough shear bands to explain all the gradual changes in dip of bedding on the Gullfaks Field by shear bands alone. For instance, dipmeter data show that 63% of all faults are associated with a zone of local drag. The average width of this local drag zone (as measured along the well bore path) is 60 m in the hanging wall and 29 m in the footwall. This is much wider than the average width of the zone affected by shear bands (19 m), and some of the drag-related shearing must have occurred by a different mechanism. In addition, the average total displacement caused by shear bands in cores containing larger-scale faults (>6.5 m missing section) is only 1.7 m (this accounts for all shear bands in the well, not

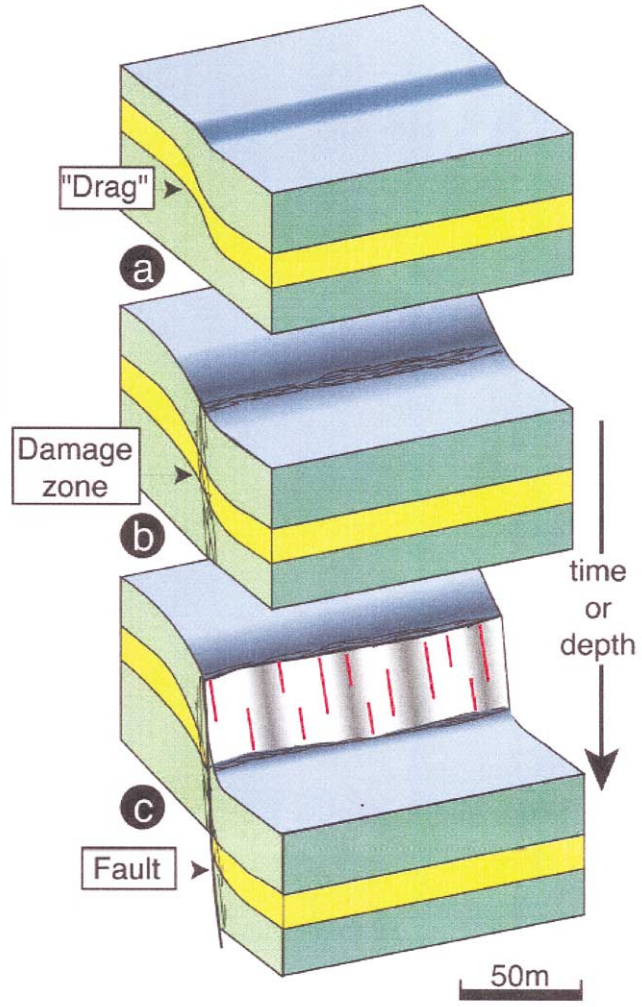

Fig. 18. Development of fault structures: (a) drag zone development; (b) formation of damage zone (shear band zone); (c) development of slip (fault) surface. (a)–(c) may be looked at as a time sequence, but also as spatial variation along a fault deformation zone, where (a) describes the situation ahead of the tip of the fault.

only those restricted to the damage zone), clearly not enough to explain the changes in bedding curvature observed from dipmeter data and core data (see Hesthammer, 1999b for detailed results from analyses of individual wells). Thus the ductile (drag) deformation was by a widely distributed translation and rotation of individual grains (granular flow) (Fossen & Hesthammer, 1998b) — a typical deformation mechanism for loosely consolidated sediments.

Although the age relation between damage zones (shear band swarms) and ductile deflection of bedding (drag) is difficult to prove, we believe that at least a certain amount of the ductile deformation precedes damage zone formation. Similarly, damage zones are at least partly considered to form prior to the main slip surface, as demonstrated from porous sandstones in Utah (Aydin & Johnson, 1978). If the slip surface is more or less planar and represents a relatively weak surface, the damage zone is not expected to grow any further. Hence, both the damage zone and the drag zone are relicts from the pre-faulting deformation history. However, any complication during fault slippage that may be generated by non-planar fault surfaces or changing boundary conditions, may cause compatibility problems and renewed growth of the damage zone and/or drag zone. Thus, a large scatter in displacement–damage zone width diagrams (as seen in Fig. 12) is expected.

6.4. Implications for models of reservoir performance

The results from structural core analyses provide important input for reservoir development. For instance, comparison of core data and seismic attribute data revealed that areas on the timedip maps with numerous (curvi-)linear features are in fact areas of poor seismic data quality rather than areas of high structural complexity. In general, poor data quality represents a problem along the crest of the Gullfaks and Gullfaks Sør fields and the crests of the rotated

domino fault blocks where gas has entered the cap rocks, thus reducing the signal-to-noise ratio. Since each of the faults in the Gullfaks area contains a damage zone with numerous shear bands that tend to restrict fluid flow, areas of high fault density should be avoided when drilling producers and injectors. If the (curvi-)linear features observed on seismic attribute maps were believed to represent faults, the crest of rotated fault blocks may have been considered unfavourable drilling sites for producers, possibly leading to non-optimal field development.

Results from structural core analyses are commonly used to estimate fault sealing potential in order to improve models for reservoir performance (Hesthammer & Fossen, 2000). For instance, known fault rock properties (Manzocchi, Walsh, Nell, & Yielding, 1999; Yielding, Freeman, & Needham, 1997; Yielding, Øverland, & Byberg, 1999) can be combined with fault juxtaposition diagrams (Allan, 1989; Knipe, 1997) to evaluate the sealing potential of faults. The input is generally based on displacement estimates from seismic interpretation, known rock properties and the general relationship between fault deformation zone thickness and displacement. The effect of shear bands within and outside the damage zone (not the entire fault deformation zone) is generally not considered.

The following discusses how several of the existing uncertainties associated with fault sealing analyses and reservoir models can be reduced by implementing results from the core analyses carried out in the Gullfaks area. However, although detailed geometrical and petrophysical studies of deformation characteristics associated with faults will help optimise existing tools for modelling reservoir performance, many uncertainties still exist and cannot be solved by analyses of well data and seismic data alone. The rapid subseismic spatial changes in continuity and geometry along faults, including the presence of relay structures, will always represent a serious uncertainty for simulations of fluid flow in reservoirs. For instance, Foxford et al. (1998) concluded from studies of the Moab Fault in Utah that the fault structures cannot be predicted over distances greater than 10 m. Furthermore, the geometry of deformation bands inside and outside of the damage zones can only partially be extracted from the core data. Lateral changes in geometry (interaction with other deformation bands and length–displacement relationships) can only be resolved by studying outcrop data and will represent large uncertainties depending on how closely the outcrop data match those within the reservoir. In general, it should not be assumed that shear bands have similar displacement–length ratios as faults with discrete slip planes. Studies from Utah (Fossen & Hesthammer, 1997, 1998b) show that deformation bands can be as much as three orders of magnitude longer than faults with discrete slip surfaces (assuming similar displacement). However, there are significant differences between deformation bands in Utah and those in the Gullfaks Field. Deformation bands in Utah developed after the rocks were consolidated and the bands are therefore highly affected by cataclasis. The reservoir rocks on Gullfaks Field, on the other hand, were less consolidated at the time of deformation and the deformation bands are therefore mainly associated with disaggregation structures. As such, different displacement–length relationships must be expected related to shear bands from the two areas.

Since these uncertainties cannot be resolved by results from the present study, we believe that efforts to demonstrate how the analyses have resulted in a better prediction of fault sealing potential would mislead the reader. Instead, the analyses aim to enhance the readers understanding of the structural reservoir characteristics and the uncertainties associated therein. This knowledge should be used to critically evaluate results from existing modelling tools. For the builders of such tools, the following results should at least help to improve the models, although the results must still be treated with care (see also Hesthammer & Fossen, 2000 for further details on this topic).

A total of 4824 shear bands were identified from structural core analyses in the Gullfaks area. The average displacement along each of them is 8.61 mm. This gives a total offset of 42 m. Although the measurements of average displacement are somewhat inaccurate (since the measurements from the slabbed core surfaces do not represent true displacement and the core is unlikely to penetrate the shear band where the maximum displacement is located), it gives a rough estimate of the total displacement accommodated by the shear bands.

Fig. 11 demonstrates that all faults are associated with a narrow damage zone consisting of abundant shear bands. The width of the damage zone is generally less than 20 m for faults with displacement less than 15–20 m and 20–80 m for faults larger than 15–20 m. The average number of shear bands associated with the faults can be calculated from the fracture frequency diagrams (Fig. 11; average of 124 shear bands associated with faults smaller than 20 m and 312 shear bands associated with faults larger than 20 m), although the individual variations are large and will represent serious uncertainties for individual fault sealing potential estimates. The width of the shear bands depends on grain size (average of 0.51 mm for very fine sandstone and 3.47 mm for very coarse sandstone) and mica content (average of 1.04 mm for equal amounts of mica and quartz and 1.95 mm for clean quartz sandstone; Fig. 8), which is known from well logs and sedimentary core studies. The reduction in permeability depends on the content of phyllosilicates and the exact numbers are found from specific field studies. These factors can be combined in order to estimate how much fluid flow is restricted in a fault's damage zone (i.e. the zone containing abundant shear bands). This may again be combined with studies of permeability reductions related to fault zones (the fault zone is the narrow zone containing fault gouge and fault breccia; see Fig. 4c) (Allan, 1989; Bouvier, Kaars-Sijpesteijn, Kluesner, Onyejekwe, & Van der Pal, 1989; Fristad, Groth, Yielding, & Freeman, 1997; Fulljames, Zijerveld, & Franssen, 1997; Gibson, 1994, 1998; Hesthammer & Fossen,

2000; Knipe, 1992, 1993, 1997; Knott, 1993; Manzocchi et al., 1999; Ottesen Ellevset et al., 1998; Smith, 1980; Yielding et al., 1997, 1999) to provide the engineer with as accurate data as possible.

The apparent under-representation of faults with displacement in the range of 0.2–6.5 m has a positive effect on reservoir performance. Furthermore, more than 70% of the smaller shear bands are located within damage zones to larger faults. The effect depends on the ability of small faults to prevent fluid flow across them and on the thickness of reservoir sand units. In fields where deformation mechanisms involve more cataclasis and strata are thinner than in the Gullfaks reservoirs, the effect may prove to be dramatic. Application of power-law relationships between displacement and frequency for faults in such reservoirs as described by Gauthier and Lake (1993), could introduce large errors to models of reservoir performance on the Gullfaks Field. On the other hand, it is important to realise that during many reservoir considerations, shear band cluster (network) zones should be considered as single faults with a displacement similar to the sum of those of the individual shear bands. Their ability to restrict fluid flow would then depend on their internal physical properties (reduced porosity of sheared rock) rather than juxtaposition of sand/shale. In general, porosity/permeability reduction caused by sandstone deformation in shear bands seems to be modest, and the negative effect of shear band or deformation band cluster zones in the reservoir is therefore likely to be small in most cases, except where post-deformational diagenetic changes has taken place (Gullfaks Sør, see below).

As revealed by the study of host rock and fault rock hardness, there are important differences between the Gullfaks Field and Gullfaks Sør related to the degree of lithification and diagenetic processes. These differences have serious consequences for field development plans. Although the general deformation characteristics are the same, the temperatures within the reservoirs on Gullfaks Sør have exceeded the critical temperatures for accelerated quartz dissolution (120°) and precipitation and illitisation of kaolinite and K-feldspar. This has led to reduced porosity and permeability within the reservoir and the many shear bands found within damage zones around the many larger-scale faults. The shear bands are most affected by quartz dissolution reprecipitation, i.e. grain-to-grain quartz dissolution, and reprecipitation, i.e. cementation, due to infiltration of illitic clay which serves to promote dissolution between quartz grains. As a result, faults or shear bands on Gullfaks Sør restrict fluid flow in the reservoir to a much greater extent than on the Gullfaks Field because of the enhanced diagenesis.

7. Conclusions

Studies of more than 8 km of core data from the structurally complex Gullfaks area have helped to constrain the structural geology of the area. Core data provide the geologist with the most detailed information available. Results from analyses of core data can be integrated with well log data, dipmeter data and seismic data to help understand the deformation characteristics and locate erroneous data or interpretations. The detailed analyses from the Gullfaks Field have demonstrated the following:

- All faults with discrete slip surfaces on the Gullfaks Field are associated with abundant shear bands in a narrow damage zone. The width of the damage zone is generally less than 20 m for faults associated with less than 15–20 m missing section and 20–80 m for faults larger than 15–20 m. Although the individual variations are large, damage zones associated with smaller faults (<20 m missing section) generally contain several tens of shear bands, whereas damage zones to larger faults (>20 m missing section) on average contain a few hundred shear bands. Due to the large individual variations, the results should be used with care for input to models of reservoir performance.
- The fact that the vast majority of the shear bands occurs in fault damage zones or cluster zones shows that they formed during faulting. This localisation is considered to be positive for reservoir performance.
- Phyllosilicate framework structures represent the most common type of shear bands and occur in sandstones with a phyllosilicate content of more than 20–25%. Disaggregation structures are most common in cleaner sandstones. Very little cataclasis is observed.
- Reduction in permeability across shear bands depends on the amount of phyllosilicates present. For phyllosilicate-rich rocks, the reduction in permeability varies between two and four orders of magnitude. Disaggregation structures are only associated with minor reduction in permeability.
- Most of the shear bands occur within network zones (i.e. intervals of intense deformation). Isolated bands exist outside the network zones but decrease rapidly in intensity away from faults associated with discrete slip surfaces.
- The width of shear bands increases with increasing grain size. Also, shear bands in clean sandstones are wider than those in rocks containing more phyllosilicates. The widest bands are observed in clean and very coarse sandstones affected by cataclasis.
- Due to enhanced quartz dissolution and precipitation and illitisation of kaolinite and K-feldspar associated with shear bands on Gullfaks Sør, faults in this area restrict fluid flow in the reservoir to a much greater extent than on the Gullfaks Field.
- Core studies indicate that minor faults on the Gullfaks Field post-date rotation of the bedding. Both ~E and W-dipping sets of shear bands developed and initiated with an *average* minimum dip of 50°.
- Core studies demonstrate that most of the (curvi-)linear features observed on seismic attribute maps are related to noise-interference features rather than faults.

- A possibly significant under-representation or gap in fault size exists between shear bands with displacement <20 cm, and faults with displacement >6.5 m — a gap that enhances communication. This observation should be seriously considered also in similar reservoirs if subsurface faults are an issue.
- Much of the deformation in the Gullfaks Field was by a widely distributed grain reorganisation rather than by discontinuous faulting.
- Results from core analyses can improve existing models for reservoir performance by including information on permeability reduction across shear bands, average width and density of bands and width of damage zones. However, any efforts to model fluid flow in the reservoir must consider the uncertainties associated with fault and shear band geometries that cannot be resolved by seismic data or core data.

Acknowledgements

The authors thank Statoil and Norsk Hydro ASA for permission to publish the results. Roy H. Gabrielsen and two anonymous referees are thanked for constructive comments.

References

Aarland, R., & Skjerven, J. (1998). Style of deformation across a major fault cored in the Brage Field, Block 31/4, northern North Sea. In M. P. Coward, H. Johnson & T. S. Daltaban, *Structural geology in reservoir characterization. Geological Society Special Publications, vol. 127*. (pp. 209–229). London: Geological Society.

Allan, U. S. (1989). Model for hydrocarbon migration and entrapment. *American Association of Petroleum Geologists Bulletin*, *73*, 803–811.

Antonellini, M., & Aydin, A. (1994). Effect of faulting on fluid flow in porous sandstones: petrophysical properties. *American Association of Petroleum Geologists Bulletin*, *78*, 355–377.

Antonellini, M., & Aydin, A. (1995). Effect of faulting on fluid flow in porous sandstones: geometry and spatial distribution. *American Association of Petroleum Geologists Bulletin*, *79*, 642–671.

Antonellini, M., Aydin, A., & Pollard, D. D. (1994). Microstructure of deformation bands in porous sandstones at Arches National Park, Utah. *Journal of Structural Geology*, *16*, 941–959.

Aydin, A. (1978). Small faults formed as deformation bands in sandstone. *Pure and Applied Geophysics*, *116*, 913–930.

Aydin, A., & Johnson, A. M. (1978). Development of faults as zones of deformation bands and as slip surfaces in sandstones. *Pure and Applied Geophysics*, *116*, 931–942.

Aydin, A., & Johnson, A. M. (1983). Analysis of faulting in porous sandstones. *Journal of Structural Geology*, *5*, 19–31.

Bengtson, C. A. (1981). Statistical curvature analysis techniques for structural interpretation of dipmeter data. *American Association of Petroleum Geologists Bulletin*, *65*, 312–332.

Bouvier, J. D., Kaars-Sijpesteijn, C. H., Kluesner, D. F., Onyejekwe, C. C., & Van der Pal, R. C. (1989). Three-dimensional seismic interpretation and fault sealing investigations, Nun River Field, Nigeria. *American Association of Petroleum Geologists Bulletin*, *73*, 1397–1414.

Fossen, H., & Hesthammer, J. (1997). Geometric analysis and scaling relations of deformation bands in porous sandstone. *Journal of Structural Geology*, *19*, 1479–1493.

Fossen, H., & Hesthammer, J. (1998a). Structural geology of the Gullfaks Field. In M. P. Coward, H. Johnson & T. S. Daltaban, *Structural geology in reservoir characterization. Geological Society Special Publications. vol. 127*, (pp. 231–261). London: Geological Society.

Fossen, H., & Hesthammer, J. (1998b). Deformation bands and their significance in porous sandstone reservoirs. *First Break*, *11*, 608–623.

Fossen, H., & Hesthammer, J. (2000). Possible absence of small faults in the Gullfaks Field, northern North Sea: implications for downscaling of faults in some porous sandstones. *Journal of Structural Geology*, *22*, 851–863.

Fossen, H., & Rørnes, A. (1996). Properties of fault populations in the Gullfaks Field, northern North Sea. *Journal of Structural Geology*, *18*, 179–190.

Fowles, J., & Burley, S. (1994). Textural and permeability characteristics of faulted, high porosity sandstones. *Marine and Petroleum Geology*, *16*, 21–25.

Foxford, K. A., Walsh, J. J., Watterson, J., Garden, I. R., Guscott, S. C., & Burley, S. D., 1998. Structure and content of the Moab Fault Zone, Utah, USA, and its implication for fault seal predictions. In: G. Jones, Q. J. Fisher & R. J. Knipe, *Faulting, Fault Sealing and Fluid Flow in Hydrogen Reservoirs. Geological Society Special Publications, vol. 147* (pp. 87–103).

Fristad, T., Groth, A., Yielding, G., & Freeman, B. (1997). Quantitative fault seal prediction — a case study from the Oseberg Syd. In P. Møller-Pedersen & A. G. Koestler, *Hydrocarbon seals: importance for exploration and production. Norwegian Petroleum Society Special Publication*, *vol. 7,* (pp. 107–124).

Fulljames, J. R., Zijerveld, J. J., & Franssen, C. M. W. (1997). Fault seal processes: systematic analysis of fault seals over geological and production time scales. In P. Møller-Pedersen & A. G. Koestler, *Hydrocarbon seals: importance for exploration and production. Norwegian Petroleum Society Special Publication, vol. 7*, (pp. 51–59).

Færseth, R. B., Sjøblom, T. S., Steel, R. J., Liljedahl, T., Sauar, B. E., & Tjelland, T. (1995). Tectonic controls on Bathonian–Volgian syn-rift successions on the Visund fault block, northern North Sea. In R. J. Steel, et al., *Sequence stratigraphy on the Northwest European margin. NPF Special Publication, vol. 5*, (pp. 325–346).

Gabrielsen, R. H., & Aarland, R.-K. (1990). Characteristics of pre- and syn-consolidation structures and tectonic joints and microfaults in fine to medium-grained sandstones. In N. Barton & O. Stephansson, *Rock joints* (pp. 45–50). Rotterdam: Balkema.

Gabrielsen, R. H., Aarland, R.-K. (1995). How can fracture analysis contribute to the understanding of previous and recent stress systems? In A. Myrvang, M. Fejerskov (Eds.), *Proceedings of the Workshop on Rock Stresses in the North Sea*, Trondheim (pp. 38–48).

Gabrielsen, R. H., Aarland, R.-K., & Alsaker, E. (1998). Identification and spatial distribution of fractures in porous, silicalastic sediments. In M. P. Coward, H. Johnson & T. S. Daltaban, *Structural geology in reservoir characterization. Geological Society Special Publications, vol. 127,* (pp. 49–64). London: Geological Society.

Gabrielsen, R. H., Færseth, R. B., Steel, R. J., Idil, S., & Kløvjan, O. S. (1990). Architectural styles of basin fill in the northern Viking Graben. In D. J. Blundell & A. D. Gibbs, *Tectonic evolution of the North Sea rifts* (pp. 158–179). Oxford: Clarendon Press.

Gabrielsen, R. H., & Kløvjan, O. S. (1997). Late Jurassic–early Cretaceous caprocks of the southwestern Barents Sea: fracture systems and rock mechanical properties. In P. Møller-Pedersen & A. G. Koestler, *Hydrocarbon seals: importance for exploration and production. NPF Special Publication, vol. 7,* (pp. 73–89). Singapore: Elsevier.

Gabrielsen, R. H., & Koestler, A. G. (1987). Description and structural implications of fractures in late Jurassic sandstones of the Troll Field, northern North Sea. *Norsk Geologisk Tidsskrift*, *67*, 371–381.

Gauthier, B. D. M., & Lake, S. D. (1993). Probablistic modeling of faults below the limit of seismic resolution in Pelican Field, North Sea, offshore United Kingdom. *American Association of Petroleum Geologists Bulletin*, *77*, 761–777.

Gibson, R. G. (1994). Fault-Zone seals in siliclastic strata of the Columbus

Basin, offshore Trinidad. *American Association of Petroleum Geologists Bulletin*, *78*, 1372–1385.

Gibson, R. G. (1998). Physical character and fluid-flow properties of sandstone-derived fault gouge. In M. P. Coward, H. Johnson & T. S. Daltaban, *Structural geology in reservoir characterization. Geological Society Special Publications, vol. 127,* (pp. 83–97). London: Geological Society.

Harper, T. R., Lundin, E. R. (1997). Fault seal analysis: reducing our dependence on empiricism. In: *Hydrocarbon seals — importance for exploration and production*. Amsterdam: Elsevier.

Harris, J. F., Taylor, G. L., & Walper, J. L. (1960). Relation of deformational fractures in sedimentary rocks to regional and local structure. *American Association of Petroleum Geologists Bulletin*, *44*, 1853–1873.

Hesthammer, J. (1998). Integrated use of well data for structural interpretation of seismic data. *Petroleum Geoscience*, *4*, 97–109.

Hesthammer, J. (1999a). Improving seismic data for detailed structural interpretation. *The Leading Edge*, *18*, 226–247.

Hesthammer, J. (1999b). *Analysis of fault geometry and internal fault block deformation in the Gullfaks region, northern North Sea*. Unpublished PhD thesis, University of Bergen, Norway.

Hesthammer, J., & Fossen, H. (1997a). Seismic attribute analysis in structural interpretation of the Gullfaks Field, northern North Sea. *Petroleum Geoscience*, *3*, 13–26.

Hesthammer, J., & Fossen, H. (1997b). The influence of seismic noise in structural interpretation of seismic attribute maps. *First Break*, *15*, 209–219.

Hesthammer, J., & Fossen, H. (1998). The use of dipmeter data to constrain the structural geology of the Gullfaks Field, northern North Sea. *Marine and Petroleum Geology*, *15*, 549–573.

Hesthammer, J., & Fossen, H. (2000). Uncertainties associated with fault sealing analysis. *Petroleum Geoscience*, *6*, 37–45.

Hesthammer, J., & Henden, J. O. (2000a). Information on fault orientation from unoriented cores. *American Association of Petroleum Geologists Bulletin*, *84*, 472–488.

Hesthammer, J., & Henden, J. O. (2000b). Closing the gap between theory and practice in seismic interpretation of small scale faults. *Petroleum Geoscience*, *6*, 107–111.

Hesthammer, J., Johansen, T. E. S., & Watts, L. (2000). Spatial relationships within fault damage zones in sandstone. *Marine and Petroleum Geology*, *17*, 837–893.

Hesthammer, J., & Løkkebø, S. M. (1997). Combining seismic surveys to improve data quality. *First Break*, *15*, 103–115.

Huang, Q., & Angelier, J. (1989). Fracture spacing and its relation to bed thickness. *Geological Magazine*, *126*, 355–362.

Jamison, W. R. (1982). Tectonic deformation of Wingate Sandstone, Colorado National Monument. *American Association of Petroleum Geologists Bulletin*, *66*, 2584–2608.

Knipe, R. J. (1992). Faulting processes and fault seal. In R. M. Larsen, *Structural and tectonic modelling and its application to petroleum geology* (pp. 231–261). Stavanger: NPF (Norwegian Petroleum Society).

Knipe, R. J. (1993). The influence of fault zone processes and diagenesis on fluid flow. In A. D. Horbury & A. G. Robinson, *Diagenesis and basin development. AAPG Studies in Geology, vol. 36,* (pp. 135–154). American Association of Petroleum Geologists.

Knipe, R. J. (1997). Juxtaposition and seal diagrams to help analyze fault seals in hydrocarbon reservoirs. *American Association of Petroleum Geologists Bulletin*, *81*, 187–195.

Knott, S. D. (1993). Fault seal analysis in the North Sea. *American Association of Petroleum Geologists Bulletin*, *77*, 778–792.

Ladeira, F. L., & Price, N. J. (1981). Relationships between fracture spacing and bed thickness. *Journal of Structural Geology*, *3*, 179–183.

Manzocchi, T., Walsh, J. J., Nell, P., & Yielding, G. (1999). Fault transmissibility multipliers for flow simulation models. *Petroleum Geoscience*, *5*, 53–63.

Needham, T., Yielding, G., & Fox, R. (1996). Fault population description and prediction using examples from the offshore U.K. *Journal of Structural Geology*, *18*, 155–167.

Ottesen Ellevset, S., Knipe, R. J., Olsen, T. S., Fisher, Q. T., & Jones, G. (1998). Fault controlled communication in the Sleipner Vest Field, Norwegian Continental Shelf: detailed, quantitative input for reservoir simulation and well planning. In G. Jones, Q. J. Fisher & R. J. Knipe, *Faulting, fault sealing and fluid flow in hydrocarbon reservoirs. Geological Society Special Publications, vol. 147.* (pp. 283–297). London: Geological Society.

Pittman, E. D. (1981). Effect of fault-related granulation on porosity and permeability of quartz sandstones, Simpson Group (Ordovician), Oklahoma. *American Association of Petroleum Geologists Bulletin*, *65*, 2381–2387.

Roberts, A. M., Yielding, G., & Badley, M. E. (1990). A kinematic model for the orthogonal opening of the Late Jurassic North Sea rift system, Denmark–Mid Norway. In D. J. Blundell & A. D. Gibbs, *Tectonic evolution of the North Sea rifts* (pp. 180–199). Oxford: Clarendon Press.

Rolph, T. C., Shaw, J., Harper, T. R., & Hagan, J. T. (1995). Viscous remanent magnetisation: a tool for orientation of rock core. In Turner & Turner, *Palaeomagnetic applications in hydrocarbon exploration and production. Geological Society Special Publications, vol. 98.* (pp. 239–243). London: Geological Society.

Smith, D. A. (1980). Sealing and non-sealing faults in Lousiana Gulf Coast Salt Basin. *American Association of Petroleum Geologists Bulletin*, *64*, 145–172.

Tollefsen, S., Graue, E., & Svinddal, S. (1994). Gullfaks development provides challenges. *World Oil*, *94*, 45–54.

Underhill, J. R., & Woodcock, N. H. (1987). Faulting mechanism in high-porosity sandstones: New Red Sandstone, Arran, Scotland. In M. E. Jones & R. M. F. Preston, *Deformation of sediments and sedimentary rocks*. *Geological Society Special Publication, vol. 29,* (pp. 91–105). London: Geological Society.

Wibberley, C. A. J., Petit, J-P., & Rives, T. (1999). Mechanics of high displacement gradient faulting prior to lithification. *Journal of Structural Geology*, *21*, 251–257.

Yielding, G., Freeman, B., & Needham, D. T. (1997). Quantitative fault seal prediction. *American Association of Petroleum Geologists Bulletin*, *81*, 897–917.

Yielding, G., Øverland, J. A., & Byberg, G. (1999). Characterization of fault zones for reservoir modeling: an example from the Gullfaks Field, northern North Sea. *American Association of Petroleum Geologists Bulletin*, *83*, 925–951.